PARTIAL CRYSTALLIZATION BEHAVIOR OF IRON BASED GLASS-COATED AMORPHOUS METAL

BY

MORGAN D. CONKLIN

A THESIS
SUBMITTED TO THE FACULTY OF

ALFRED UNIVERSITY

IN PARTIAL FULFILLMENT OF THE REQUIREMENTS
FOR THE DEGREE OF

MASTER OF SCIENCE

IN

GLASS SCIENCE

ALFRED, NEW YORK

AUGUST, 2004

PARTIAL CRYSTALLIZATION BEHAVIOR OF IRON BASED GLASS-COATED AMORPHOUS METAL MICRO-WIRES

BY

MORGAN D. CONKLIN

B.S. ALFRED UNIVERSITY (2002)

SIGNATURE OF AUTHOR (Signature on file)

APPROVED BY (Signature on file)
WILLIAM C. LaCOURSE, ADVISOR

(Signature on file)
ALEXIS CLARE, ADVISORY COMMITTEE

(Signature on file)
XINGWU WANG, ADVISORY COMMITTEE

(Signature on file)
DOREEN EDWARDS, CHAIR, ORAL THESIS DEFENSE

ACCEPTED BY (Signature on file)
ALASTAIR CORMACK, DEAN,
SCHOOL OF ENGINEERING

ACKNOWLEDGMENT

Graduate school is difficult, as it should be. A student should be challenged to work and grow beyond his or her previous limits in a manner that is sometimes less than comfortable. While I do not deny working through this challenge, my graduate experience was difficult for other reasons as well. Illness, poor health, depression, anxiety, and bad habits all conspired to make my life miserable. On the other hand, the people I have lived and worked with through the duration have afforded me some of the richest and enjoyable times of my life. For this, I thank them all, for tempering the bad times and helping me succeed.

I thank my advisor Dr. William LaCourse for his guidance, my committee members Dr. Clare and Dr. Wang, all the faculty and staff at Alfred, and all my classmates over the past 6 years. Also thanks to all of my friends and family, who would never have let me let them down.

Morgan

Table of Contents

Page

Acknowledgments iii

Table of Contents iv

List of Tables vi

List of Figures vii

Abstract ix

I INTRODUCTION 1

A. Glass Coated Amorphous Metal 1

1. Manufacture 2

B. Properties 4

1. Electrical Properties 4

2. Magnetic Properties 4

a) Magnetostriction 5

b) Giant Magneto-Impedance 5

c) Large Barkhausen Effect 6

3. Mechanical Properties 6

C. Uses and Applications 7

1. Magnetics 7

2. Mechanical 8

3. Electrical 8

4. Sensors 8

5. Actuators and Susceptors 8

6. Glass Covering 9

D. Iron Boron Silicon Core Composition 10

II EXPERIMENTAL PROCEDURE 12

A. Crystallization Separation 12

E. Determination of Activation Energies 14

1. Kissinger's Analysis 15

2. Differential Scanning Calorimetry 17

F. Thermo-Magneto-Gravimetry 20

G. Resistive Heating 23

H. Magnetic Harmonic Resonance 26

I. Strength Testing 28

J. Handling, Preparation, and Safety 30

K. Scanning Electron Microscopy 31
III DISCUSSION 38
A. Core-Cladding Separation 38
B. Double Crystallization 39
IV SUMMARY AND CONCLUSIONS 40
A. Crystallinity and Mechanical Strength 40
B. Nano-Crystallinity 40
C. Resistive Heating 40
D. Magnetic Resonance 41
E. Future Work 41
REFERENCES 42

.

LIST OF TABLES

Page

Table I. Measured Crystallization Temperatures for Iron-Based GCAM.....17

Table II. Calculated Estimates of Activation Energies for GCAM Wires 18

Table III. Curie Temperatures of GCAM Samples 22

Table IV. Ratio of Iron to Silicon X-ray Count Peaks.....36

LIST OF FIGURES

Page

Figure 1. Structure of Glass-Coated Amorphous Metal fiber. 2

Figure 2. Schematic of the fiber draw process. 3

Figure 3. DSC plot of iron based GCAM, with two exothermic crystallization peaks. 10

Figure 4. The change in secondary crystallization as a function of heat treatment hold times. 13

Figure 5. Diagram of alumina sample holder used during heat treatment. 14

Figure 6. DSC curves for iron fiber composition showing peak shifts between different heating rates. 18

Figure 7. A Kissinger plot for the secondary crystallization peak of iron based GCAM. 19

Figure 8. Schematic of a thermo-magneto gravimetric device. 20

Figure 9. A Thermo-Magneto-Gravimetric curve showing the manetization of GCAM fiber over a temperature range covering the Curie temperature, and crystallization. 21

Figure 10. TMG curve for CoFeSiB fiber showing no return to ferromagnetism after crystallization. 22

Figure 11. Schematic of the resisive heating apparatus. 24

Figure 12. Graph shoing the linear change in length with power dissipated in fiber. 25

Figure 13. Expansion curve of CoFeSiB composition against power input. 26

Figure 14. Diagram of the harmonic analysis setup. 27

Figure 15. Bar graph showing the magnetic harmonic response of $Fe_{77.5}Si_{7.5}B_{15}$ composition GCAM fiber at 1kHz. 28

Figure 16. Weibull plot for FeSiB fiber, semi-crystalline and as-received. 29

Figure 17. SEM micrograph of a sulfuric acid treated fiber. 32

Figure 18. SEM micrograph showing GCAM fiber cross-sections. 33

Figure 19. Images of the cores of semi-crystalline fibers, showing nanoscale structure. 34

Figure 20. EDS spectrum of FeSiB composition fiber. 35

Figure 21. Normal and BSE images showing separation of the metal core from the glass, and backfilling with polishing burr. 37

ABSTRACT

Thermal and physical properties of glass-coated amorphous metal fibers have been investigated. It is demonstrated that an amorphous metal having a composition of $Fe_{77.5}Si_{7.5}B_{15}$ undergoes a two-stage crystallization process when heated, and that the lower temperature crystallization can be completed without the higher temperature crystallization occurring. Scanning electron microscopy shows that such "Partial-Crystallization" creates a nanocrystalline, apparently interconnected structure within an amorphous matrix. The activation energy for the lower and upper temperature crystallizations have been calculated to be approximately 424 kJ/mol and 361 kJ/mol, respectively, using differential scanning calorimetry and Kissinger's analysis. Crystallization temperature is heating rate dependant; at 10 ºC per minute, the two crystallizations occur at 540.5ºC and 550.5ºC respectively. Using a programmable dental furnace, a sample can be subjected to a heating curve and quenched in air, causing only the first crystallization to occur. The material so prepared is shown to have properties distinguished from the as-received material. The ultimate tensile strength of a partially crystallized fiber is measured to be 10-40% weaker than that of an as received sample. A core composition of $Co_{68.15}Fe_{4.35}Si_{12.5}B_{16}$ has also been tested and has a single crystallization temperature (at 10ºC/min) of 552ºC with an activation energy of 503 kJ/mol. Using thermo-magneto-gravimetric analysis, Curie temperatures have been measured for the amorphous metal compositions; 426ºC for $Fe_{77.5}Si_{7.5}B_{15}$, and 319ºC for $Co_{68.15}Fe_{4.35}Si_{12.5}B_{16}$.

I INTRODUCTION

Amorphous metals constitute a fascinating class of materials with many unique mechanical, electric, and magnetic properties. Sometimes referred to metallic glasses, or glassy metals, these materials have a randomized atomic structure which is analogous to that of the liquid phase of the alloy, similar to the structural character observed in glass. In order to form a metal with an amorphous structure however, it must be solidified from the liquid state rapidly enough to outpace the crystallization kinetics of the melt, thus preserving the random atomic structure of the liquid. Fundamental to the process is the so called "confusion principle," which holds that the more dissimilar types of atoms present in the melt, the more difficult it will be for the atoms to arrange themselves into a crystalline structure upon solidification, slowing the kinetics of crystallization. This important concept is central to the design of alloys capable of forming a glass at reasonable cooling rates.

The fast cooling required puts significant limitations on the formation processes and the physical geometry of the materials. To maximize the heat transfer between the metal and the quenching medium, the ratio of surface area to volume of the melt must be very high. One common method is to pour an alloy melt onto a flywheel rotating at high speed, causing a continuous ribbon of amorphous metal to be produced. The more primitive splat cooling technique develops sufficient cooling rates, wherein a molten drop is allowed to fall onto a heat sink, but this produces a material with critical limits on geometry and is not typically used for production. The "in-rotating-water" method spins wires of amorphous alloy from the melt while in a bath of water, which serves as the quenching element. Alternative methods of amorphous metal production that do not involve quenching a melt include sputter-coated amorphous metallic thin films, and chemically derived amorphous metal powders.

A. Glass Coated Amorphous Metal

Yet another way of obtaining such high cooling rates is to melt the source alloy within a glass tube and draw away a continuous fiber with a composite structure

consisting of an amorphous metal core surrounded by a glass cladding,[1,2] as illustrated in Figure 1.

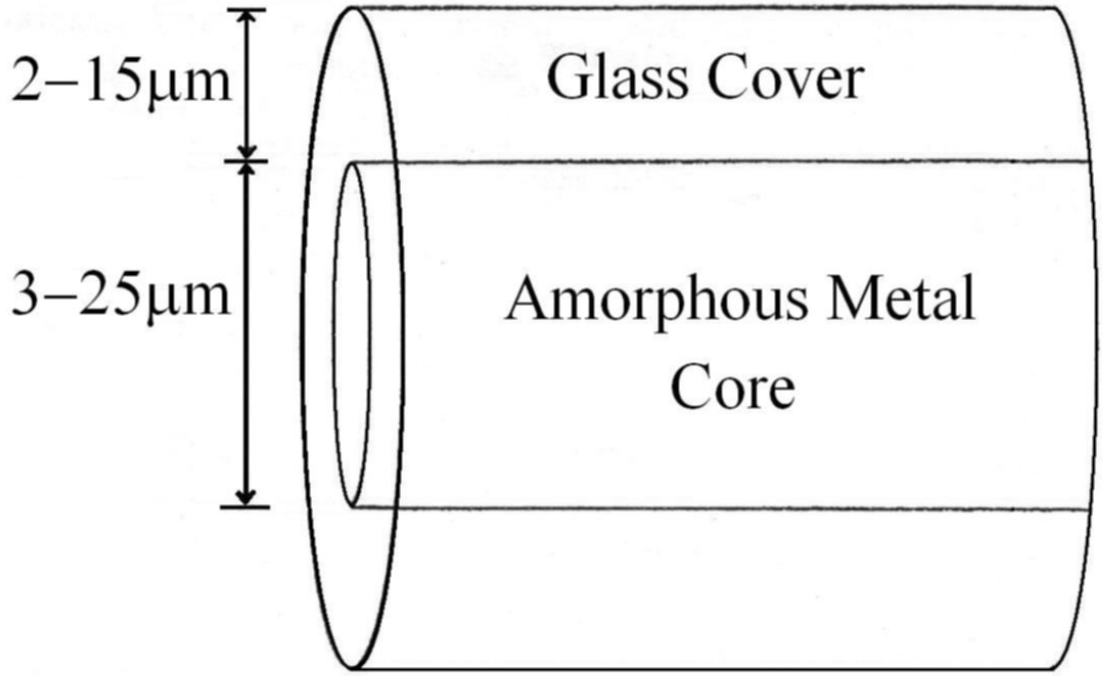

Figure 1. Structure of Glass-Coated Amorphous Metal fiber.

Such composite fibers are termed glass-coated amorphous metal (GCAM) fibers, having a diameter on the order of 10-50μm, although wires <10μm can be produced. Recent research in GCAM materials has demonstrated that due to the glass covering and the internal stresses inherent to the processing method, the magnetic character of the composite wires demonstrates some very unique and interesting properties.[1-4] Because of these composite properties, GCAM fibers show vast potential for use in sensor applications,[5] security systems, and micro-mechanics.

1. Manufacture

The glass coated melt spinning technique was developed in the early 1920's by Taylor[6] to fabricate crystalline metal cored wires, but was not used to produce amorphous material until Wiesner and Schneider did so in 1974.[7] The modern process used to produce GCAM wires has been refined by Chiriac.[1,2] A tube of glass with a Pyrex type composition is closed off at one end, and the source alloy metal is deposited inside. The

tube is then mounted in a feed mechanism which works at a speed of 0.5-7 mm-min^{-1} to replenish the glass being consumed. The open end of the tube is placed under vacuum and/or backfilled with an inert gas to prevent high temperature oxidation of the metal melt. The heating element consists of a high frequency coil which melts the alloy by magnetic induction. The molten drop of metal subsequently softens the glass tube, allowing a wire to be drawn. At about 1cm below the hot zone, a jet of water is positioned to quench the material, which is then wound onto spools. The schematic of the draw process is shown in Figure 2.

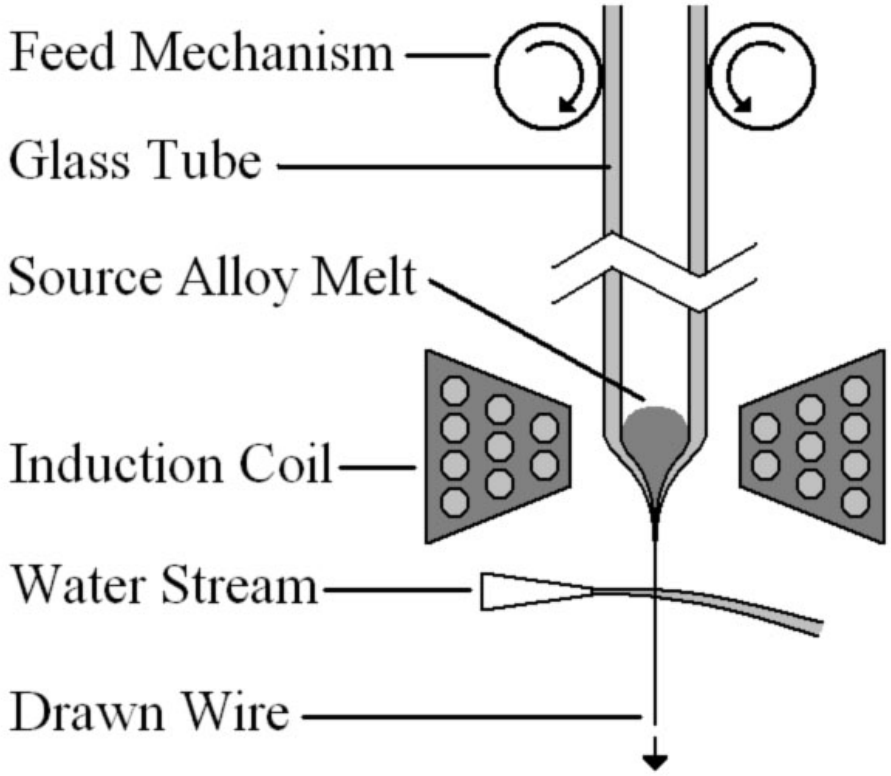

Figure 2. Schematic of the fiber draw process.

In order for this technique to be employed successfully, the material compositions must be chosen carefully, so that the melting point of the metal and the working temperature of the glass are approximately the same, with the working range of the glass somewhat above the T_g of the alloy. The thermal expansions of the glass and the amorphous core must be relatively close to prevent catastrophic failure from thermal shock, but the core should have a higher expansion coefficient so that the thermal stresses

that do develop will put the glass cladding under compression in the finished wire. Moreover, the viscosity of the glass over a range of temperatures should be taken into account, as it will impact drawing rates. The drawing rate of the fiber necessarily influences the final geometry of the wire, along with the initial geometry of the glass tube which retains its initial ratios of diameters and wall thickness during the draw process.

Chemical interactions between the alloy and the glass are also important, especially at the high temperatures required by the process. The wires being investigated have a core composition containing iron, boron, and silicon; the latter two being components in the alumino-borosilicate composition of the glass tube, and iron is a common contaminant in silica and derivative glasses. Additionally, the thermodynamics of interaction between the material compositions dictate the surface energy and contact angles of the glass and the metal melt.

B. Properties

1. Electrical Properties

Although the core of the composite wires is a metallic alloy, its amorphous quality drastically diminishes electron mobility within the material, causing the resistivity to be relatively large, on the order of 10^{-4} Ω-cm. The high resistivity, along with the very small cross section of the wire core makes the material quite resistive per unit length, about 25Ω/cm. However, the change in resistivity over a temperature range is lower than that observed in the crystalline alloy. The electrical behavior of GCAM wires is important to many of their uses, which involve the core carrying current. For instance, the resistive heating of the wires, and signals produced in the wire in sensor and antenna applications are dependant on the electrical properties, in terms of designing the circuits necessary to drive the material as an active element in such instances.

2. Magnetic Properties

The magnetic properties of GCAM composites account for a vast realm of unique material behavior and represent most of the material research focus[1-3]. To begin with, the very alloys used for the core of the wire are inherently ferromagnetic. Iron and cobalt are well known as conventional magnetic materials, and it is no coincidence that they

account for most of the core compositions produced. One of the advantages to the glass-covered drawing technique is that the extreme cooling rates that can be achieved allow the use of metal alloys that would otherwise be unable to form into amorphous materials, thus offering more flexibility in customizing the properties of the alloy through compositional variations. For the most part, this magnetic material behavior was initially established by work done with conventional amorphous wires. However, the glass coating adds another very important aspect to the magnetic properties of the amorphous metal core; the internal stresses developed upon formation of the composite. When the wire is drawn and cools, there is a mismatch between the thermal expansion coefficients of the amorphous metal and the glass cladding. The core wants to shrink much more than does the glass, causing the final product to have significant internal stresses, placing the core in tension both axially and radially. Not only is the core stressed, the small dimensions amplify the extent and magnitude of that stress throughout the core.

a) Magnetostriction

The magnetostriction of a magnetic material is the material's dimensional response to the presence of a magnetic field. It can be positive or negative depending on the material. FeSiB alloys exhibit positive magnetostriction, whereas CoSiB compositions are negative.[8,9] By controlling the levels of iron and cobalt in an alloy, a desired level of magnetostriction between the two boundaries can be developed. Smaller shifts in magnetostriction coefficient can be made by electric current annealing. Magnetostriction is also be influenced by stresses placed on the fiber, glass removal can increase the magnetostrictive value.[10]

b) Giant Magneto-Impedance

The GMI effect is the magnetic behavior where a conductive material carrying an alternating current in the 10^6-10^8Hz range experiences a radical change in resistance when placed in a static magnetic field, with resistance increases of 600% possible.[11] The GMI effect originates in the relation between magnetization of the material, and the high frequency damping of domain boundary movement. The internal stresses developed by the glass covering of GCAM fibers are detrimental to the effect, which improves markedly when the glass is removed. The GMI effect is very sensitive to fiber composition, external and internal stresses, and domain structure, and is generally seen in

material with low magnetostriction. Because of the sensitivity to stress, the GMI effect can control the use of GCAM fibers in sensors.

c) Large Barkhausen Effect

This effect is very dependant on internal stresses, and can be observed especially well in GCAM fibers.[1] The phenomenon is seen in the shape of the hysteresis curve of the material, which looks very much rectangular. This implies that the internal magnetic domain structure will respond very quickly and thoroughly to a driving magnetic field when, and only when a specific value of the coercive strength is achieved. This is in contrast to most magnetic materials, in which the switching field elicits a more smooth and varied response from the material, producing a sinusoidal hysteresis loop.

3. Mechanical Properties

As may be imagined, the mechanical behavior of the GCAM fibers is strongly dependant on the glass cladding. Like most glass, amorphous metal has no internal flaws or grain boundaries on which to initiate mechanical failure, and strength values begin to approach theoretical limits. As with tempered glass, the highly compressive stresses in the glass surface layer must be overcome before the glass will break, adding a strengthening element to the composite's tensile behavior. Additionally, the glass covering protects the core physically from mechanical abrasion damage. Since the core is under tension, the metal surface must be free of flaws that can initiate fracture. Furthermore, the outer glass layer protects the composite from chemical attack, and possible weakening. Young's modulus (tensile) of the fiber is on the order of 60-90GPa; 150GPa for the fiber core with the glass removed. Study of failure mechanisms is advantageous to designing the relative geometries of metal and glass in the composite, which helps determine the ultimate strength of the fiber.

The axial stresses developed within the fiber can be on the order of several GPa, depending on the core diameter and thickness of the glass coating. Since many properties are influenced by the internal stress, removal of the coating can change the behavior of the fiber. Glass removal can be accomplished by submerging the fiber in a bath of hydrofluoric acid (typically a 50% solution) for a short period until the glass dissolves but before the metal core begins to be corroded, and rinsed in water, or the fiber can be

dipped in liquid nitrogen, producing a thermal shock causing the glass covering to fracture and flake off. Iron based fibers are sensitive to the environment without the protective glass covering, and will rust readily.

C. Uses and Applications

With so many unique properties, it should be natural to conclude that the uses for GCAM composites be equally unique. Indeed, not only are individual applications novel in their execution, but in many instances, the possibility exists for tasks can be combined such that more than one function can be performed by the fiber at once.

1. Magnetics

Amorphous metals are already used as soft magnetic cores for high efficiency transformers and electric motors. The high resistivity values for the core materials nearly eliminate eddy currents within the metal, a main source of power loss and heat development in such devices. GCAM wires may eventually be used for this purpose in micromechanical devices, and/or those exposed to chemical environments.

GCAM fibers also offer the possibility of being encoded with digital information, through stress removal, or thermal annealing. Coded wire could then be incorporated into documents, money, or other products to prevent counterfeiting or tampering. The stored data could be read or detected with a number of levels of technology, from simple proximity detectors, to computerized decoding systems. Magnetic, microwave or radio wave scanners may be able to detect and decode fibers at a distance and out of line-of-sight, and could serve as a cost effective alternative to RFID tagging technology, which requires bulky and expensive disposable elements.

Because of the sensitivity of the magnetic character of GCAM fibers to internal and external stresses, and their inherent mechanical strength, the material could be incorporated into composites as a method of detecting and measuring internal damage or fatigue. Early detection is important in composite materials to avoid catastrophic failure, and in-situ monitoring of internal stresses would be invaluable to the design evolution process of such components.

2. Mechanical

Although somewhat more dense than typical state-of-the-art fiber reinforcements, GCAM materials have quite favorable strength and toughness parameters, and would serve as an excellent reinforcement phase, in applications where weight is not a crucial consideration. The glass coating can be engineered to be a suitable match to bonding agents, such as those already in use for use with fiberglass.

3. Electrical

Even though their high resistivity prevents GCAM wires from carrying any degree of current without heating up, there are still potential applications for use in electronics and microelectronics. Because of their sensitivity to magnetic fields, and some conductivity, amorphous metals can be used as active elements in radio aerials and other electromagnetic detection devices. As the ever-present push for miniaturization continues, GCAM wires could find a place in micro-circuitry.

The small dimensions and high resistivity might allow fibers to be used as failsafe elements or fusible links to protect against power surges in low current signal carrying circuitry.

4. Sensors

The GCAM composite fibers are particularly suited for use in sensors because of their combination of properties.[12-14] They can be imbedded, immersed, pulled, bent, twisted, heated, and so forth. Sensor devices detect changes in magnetic susceptibility, magnetic field, or measure changes in the electrical resistivity of the metal core. As previously mentioned, GCAM fibers could be incorporated into composite materials to serve as internal sensors to detect local stress environments. As such, they could act as remote sensor elements, translating physical information into a magnetic field to be scanned by external devices.

5. Actuators and Susceptors

The magnetostrictive character of the amorphous metal might be exploited by using GCAM fibers as micro-actuators, to manipulate micromechanics, or even microsurgical devices.

Because of the metal core GCAM fibers can serve as microwave susceptors. Exposed to high power microwaves, the fiber will become very hot and burn. Lower intensity exposure could remotely heat only the fiber cores.

6. Glass Covering

An ample body of research has been developed that focuses on the magnetic properties of GCAM fibers, and their use as sensor elements. Relatively little work has been done to investigate the possibilities offered by the glass covering itself. Typically, an alumino-borosilicate Pyrex-type glass is used for the covering because its high temperature properties allow for fiber formation. However, other glass compositions can be developed to work as well, that are also capable of other functionality in the final material.

Drawing on the uses of glass in the biomedical industry, some interesting applications of GCAM fibers may be possible. A Polymerase Chain Reaction, or PCR, is a process for gene replication that has driven the advance of modern genetic technology. Glass compositions are being developed that have a porous surface in which PCR can take place. If such a glass can be used in a GCAM composite, miniature gene replication devices could be developed. Even the heat required by the reaction can be supplied by running a current through the metal core. Several compositions of glass have been produced that are bioactive, capable of interacting with living tissue. Using bio-glass to form a GCAM fiber could allow its use in the body where it would otherwise be impossible.

The glass cladding might also find a role in the field of optics and photonics. Using a thicker layer of glass, or several layers of glass, the cladding would be able to support a wave-guiding condition, and carry light through its length. The magnetic metal core would be key to any unique use of the glass in photonics. Faraday rotators use a magnetic field to alter the polarization of light, a task to which a GCAM fiber might somehow be adapted. Again if application of heat is required for any reason, the resistive core can serve as a heating element.

The glass cladding can conceivably be dyed with fluorescent ions, which could be seen at only specific wavelengths of light. Coded information could be stored optically

in the glass covering, and used in conjunction with information stored magnetically within the metal core.

D. Iron Boron Silicon Core Composition

One of the alloys that can be used to make GCAM fibers is iron based, with additions of silicon and boron. The wire under study has a nominal $Fe_{77.5}Si_{7.5}B_{15}$ composition. One interesting behavior of this amorphous alloy, observed in the Fe-Si-B system when the silicon content is over 5%, is the occurrence of two crystallization phenomena, at two temperatures. Figure 3 shows a differential scanning calorimetry curve clearly showing the double crystallization.

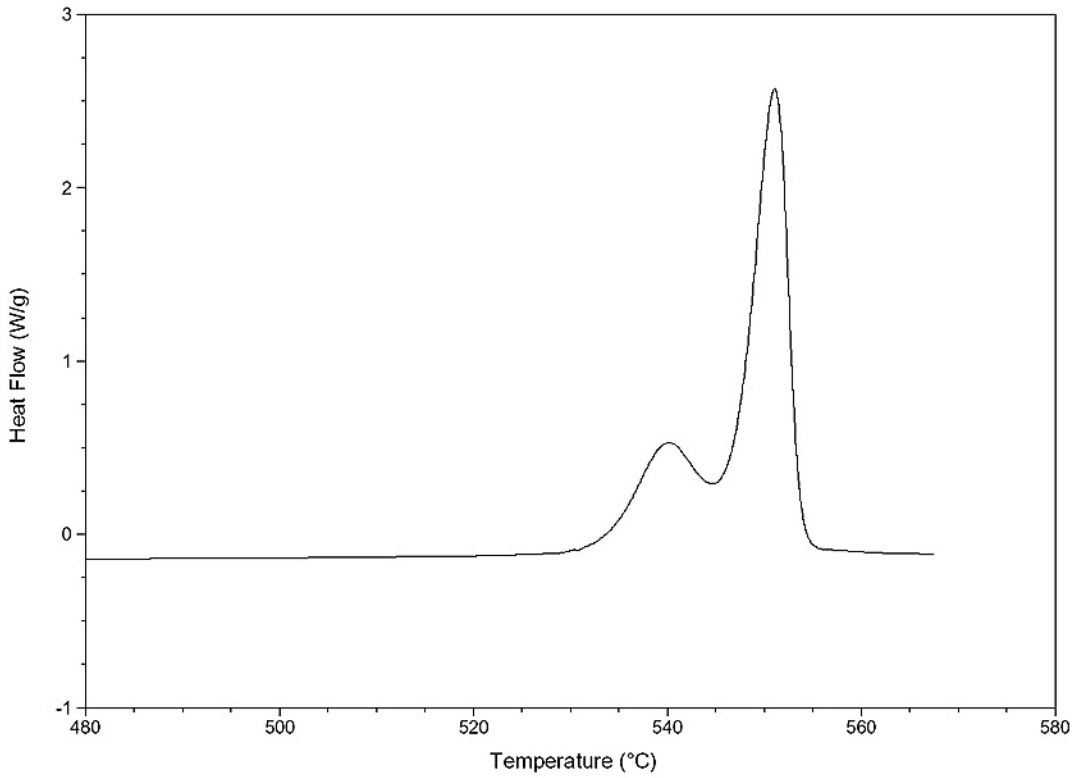

Figure 3. DSC plot of iron based GCAM, with two exothermic crystallization peaks.

Because the crystallizations occur separately, (approximately 10°C apart) it can be inferred that the phases being formed have two distinct compositions. A consequence of this in terms of exploiting the wire, is the possibility of controlling a heat treatment so

that only one crystallization occurs, leaving the balance of the material in an amorphous state. This treatment would have a significant impact on all of the properties of the material, creating new and unique opportunities for its use.

II EXPERIMENTAL PROCEDURE

Sample materials were manufactured and supplied by The National Institute of Research and Development for Technical Physics, Iasi, Romania. The compositions studied were cobalt based, $Co_{68.15}Fe_{4.35}Si_{12.5}B_{16}$; and iron based, $Fe_{77.5}Si_{7.5}B_{15}$; coated with a Pyrex®-type glass. The iron-based wire used had nominal dimensions of 36μm outer diameter, 25μm core diameter; the cobalt wire had dimensions of 40μm outer diameter, 25μm core diameter. The primary research was focused on the iron wires, and the dual crystallization behavior.

A. Crystallization Separation

The first work done to isolate the crystallization peaks was done using a DSC instrument, due to the tight control over heating curves, and the ability to monitor the process via heat flow. Samples were heated at 10°C/min to various temperatures at and below the crystallization temperatures of the material, and then quenched without holding at temperature. The same sample was then reheated to 570°C to determine the degree to which each crystallization had occurred. As the initial temperature to which the sample was heated increased, the first crystallization peak began to shrink, until approximately 520°C, when the magnitude of the first peak could be considered negligible compared to that of the second. An unexpected result was noted that as the initial crystallization peak was diminished, the second did as well to a lesser extent, and both peaks shifted to lower temperatures. The effect of hold times at temperature is shown in Figure 4. Hold times were investigated to observe the changes in secondary crystallization temperatures with respect to the degree of crystallization of the first. A similar effect would be seen among curves for differing peak temperatures, according to the degree to which crystallization has progressed.

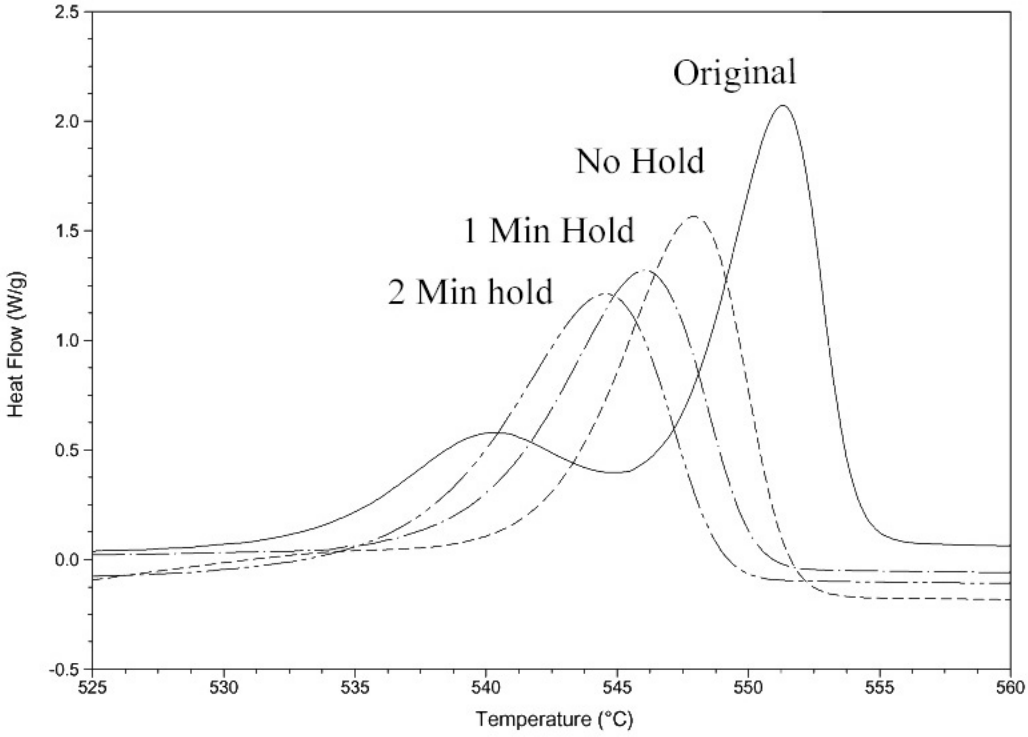

Figure 4. The change in secondary crystallization as a function of heat treatment hold times.

Although the DSC offers excellent control over heating curves, it is impossible to obtain any significant length due to the 5mm diameter sample pans. Therefore, a separate heating schedule had to be developed for use with a larger furnace. A Centurion® dental furnace was chosen for programmable function, ease of use, and a circular heating chamber. Initially, samples were heated directly in DSC sample pans to simplify the testing process. After heat treatment in the furnace, samples were transferred directly to the DSC to measure the effects of thermal process. An initial peak temperature of 520°C caused complete crystallization, and so a series of samples was run, with lowered peak temperature heating curves at intervals of 5°C, an optimum peak temperature of 490°C was determined at which the lower crystallization was mostly completed, but the upper crystallization had not begun to an appreciable degree. This thermal treatment produces samples that will be termed "semi-crystallized". Once an appropriate heating curve had been developed, continuous lengths of fiber could be partially crystallized. To do so, a sample holder was devised from a short length of alumina tubing, 4cm (diameter) x

2.5cm, (height) weighing 22 grams, with diagonal notches cut in the ends to hold the fiber, several meters of which can be wrapped around to be heated at once. Figure 5 shows a depiction of the sample holder.

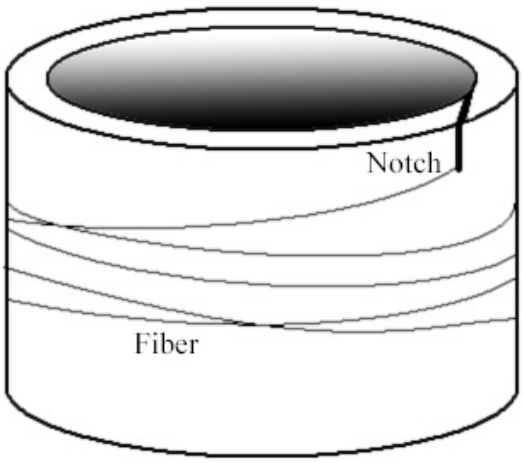

Figure 5. Diagram of alumina sample holder used during heat treatment.

All heat treatments consisted of a 10°C/min heating rate to the peak temperature with no hold time, at which point the furnace automatically opened the chamber to quench the sample in air. When using the alumina sample holder however, the extra heat capacity did not allow the material to cool quickly enough to stop the crystallization short, effectively emulating a hold time. In order to use the sample holder effectively, the maximum temperature had to be lowered to 480°C.

E. Determination of Activation Energies

The activation energy of a transformation process in a material is often determined using the Johnson-Mehl-Avrami technique, in which the fraction of the material transformed is monitored with respect to time during an isothermal heat treatment. Unfortunately, the limited dimensions of the GCAM wires would have made such an approach nearly impossible. In-situ measurement of the fraction transformed was not feasible due to the large amount of material necessary to get an X-ray diffraction signal. Heat treating the wire and quenching at time intervals would have been

prohibitively difficult as well; the small size makes the crystallization very sensitive to minor fluctuations in temperature, necessitating a sophisticated furnace and quenching system. Even then there is no suitably accurate method of determining the fraction transformed in the material. Using a JMA approach, the amount of error would have been unacceptable when compared to using a constant heating rate calculation, such as the Kissinger technique.

1. Kissinger's Analysis

Kissinger developed a method for calculating activation energy based on heating rate dependant shifts in crystallization temperature.[15,16] This approach was chosen because it has previously been used for amorphous metal crystallizations[17,18], with results in agreement with those obtained by the JMA analysis.[19,20]

Kissinger's calculations are based on some initial assumptions; that the reaction order is constant, and that it is equal to 1, (n=1) which is common for crystallization/devitricfication processes. These are used in the equation derivation, which also does not assume a nucleation and growth type mechanism.

Beginning with the assumption of a first order decomposition, the volume fraction of transformed material at a constant temperature is given by,

$$\left(\frac{\partial x}{\partial t}\right)_T = k_T(1-x) \tag{1}$$

in which x is the fraction transformed, k_T is the rate constant, and t is the time elapsed. The rate constant follows an Arrhenius relation:

$$k_T = A\exp(-\frac{E}{RT}) \tag{2}$$

where A and E are constants, frequency factor and activation energy, respectively. R is the gas constant, and T is the temperature in Kelvin.

If the temperature changes with time, the reaction rate is expressed:

$$\left(\frac{\partial x}{\partial t}\right)=\left(\frac{\partial x}{\partial t}\right)_T+\left(\frac{\partial x}{\partial T}\right)_t\frac{\partial T}{\partial t} \tag{3}$$

At a fixed time, $(\partial x/T)_t$ will be zero, because at a fixed time, the number and size of particles formed is fixed and unchanging. Therefore:

$$\left(\frac{dx}{dt}\right)=A(1-x)\exp\left(-\frac{E}{RT}\right) \tag{4}$$

provided that x and T are measured simultaneously. When the reaction rate is at a maximum, its derivative with respect to time will be equal to zero.

$$\frac{d}{dt}\left(\frac{dx}{dt}\right)=\left(\frac{dx}{dt}\right)\left(\left(\frac{E}{RT^2}\times\frac{dT}{dt}\right)-A_0\exp\left(-\frac{E}{RT}\right)\right)=0 \tag{5}$$

Because (dx/dt) must not equal zero, we can make the following statement, associating T with a temperature for the peak maximum.

$$A_0\exp\left(-\frac{E}{RT_P}\right)=\frac{E}{RT_P^2}\left(\frac{dT}{dt}\right) \tag{6}$$

The change of temperature over time (dT/dt) is the constant heating rate (Φ) in a non-isothermal experiment.

$$\ln A_0-\frac{E}{RT_P}=\ln E-\ln R-\ln T_P^2+\ln\Phi \tag{7}$$

Ignoring the constant term $\ln(A_0) - \ln(E) + \ln(R)$, which is not necessary for the determination of activation energy, the final equation becomes:

$$-\frac{E}{R} = \frac{d\ln\left(\frac{\Phi}{T_P^2}\right)}{d\left(1/T_P\right)} \tag{8}$$

Using this equation, $\ln(\Phi/T_p^2)$ is plotted against $(1/T_P)$, which yields a straight line. The slope of this Kissinger plot multiplied by (-R) gives the activation energy in Joules per mole.

2. Differential Scanning Calorimetry

To obtain crystallization temperatures experimentally, a technique is needed that can detect the small changes in heat flow associated with crystallizations, such as differential thermal analysis or differential scanning calorimetry. A TA Instruments Q10 DSC unit was used to measure crystallization temperatures in samples heated at continuous rates of 5, 10, 20 and 30°C per minute. A consolidated graph of the resultant curves is shown in Figure 6, with the corresponding peak temperatures in Table I.

Table I. Measured Crystallization Temperatures for Iron-Based GCAM

Heating Rate (°C/min)	**First Peak Temperature (± 0.1°C)**	**Second Peak Temperature (± 0.1°C)**
5	531.6	541.2
10	540.2	551.3
20	548.7	561.7
30	554.4	568.6

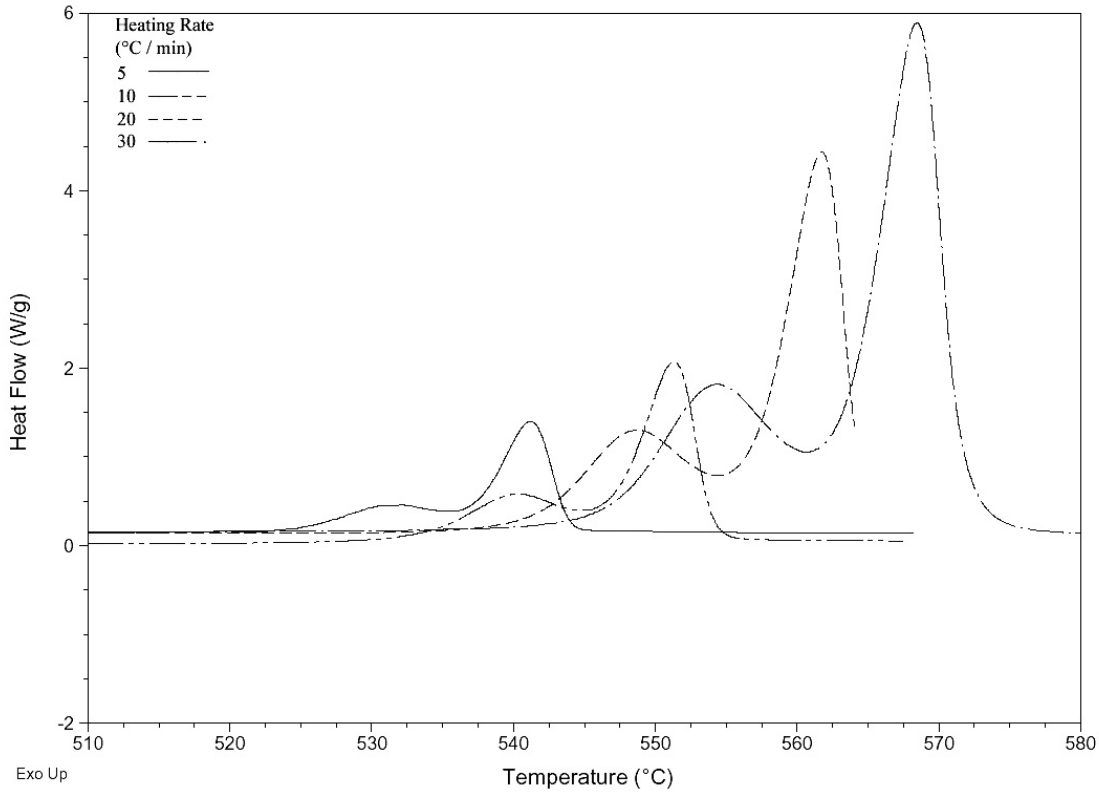

Figure 6. DSC curves for iron fiber composition showing peak shifts between different heating rates.

Samples consisted of approximately 5 mg chopped fiber encased in aluminum DSC sample pans. Peak temperatures were measured at maximum peak height, and used to develop Kissinger plots according to the equation derived above. Figure 7 shows the Kissinger plot for the second crystallization peak in the iron composition. The slope of the plot is -43360, therefore according to the derived equation, the activation for the initial crystallization is calculated to be 361kJ/mol. Experimentally determined activation energies are listed in Table II.

Table II. Calculated Estimates of Activation Energies for GCAM Wires

Sample	**Activation Energy (kJ/mol)**
FeSiB, First Peak	424
FeSiB, Second Peak	361
CoFeSiB	513

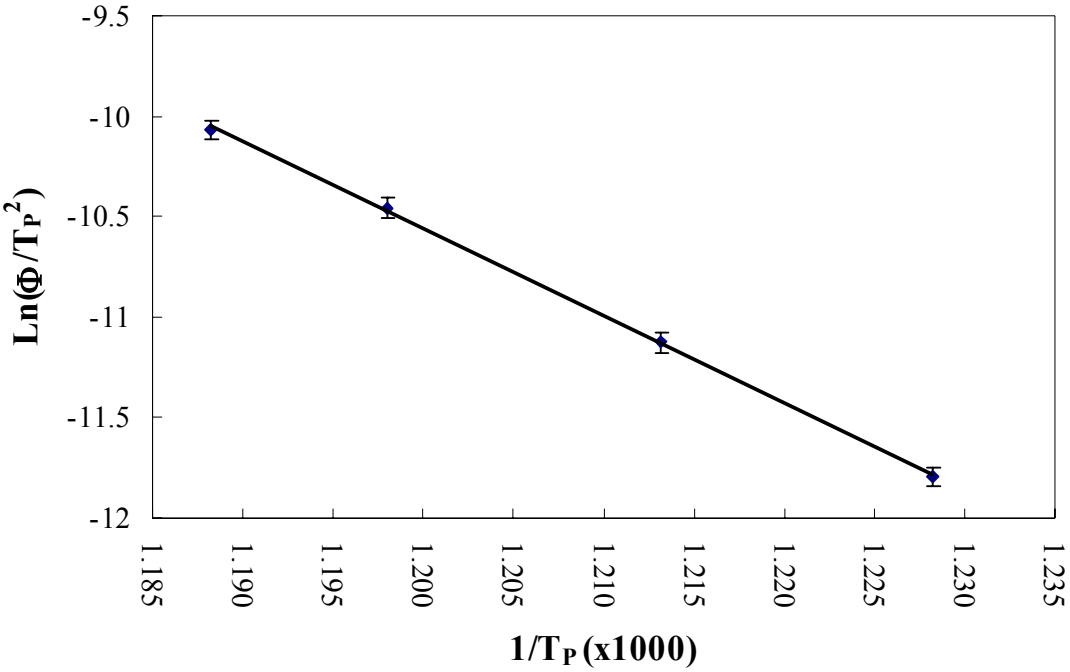

Figure 7. A Kissinger plot for the secondary crystallization peak of iron based GCAM.

Admittedly, determination of activation energies using Kissinger's technique (or any other method based on non-isothermal heating) is not inherently precise due to the assumptions that must be made about the mechanisms of the reaction. The Kissinger method for example, assumes that the reaction order and activation energy are constant, and does not consider nucleation behavior. Nevertheless, it has been shown that this technique is no less accurate than isothermal methods, and is in general agreement with the results from isothermal analysis, when used to characterize crystallizations in amorphous metal.

The activation energies for the cobalt based fiber were calculated for somewhat lower heating rates, because at higher rates, the crystallization peak begins to split into two peaks, much like the iron composition.

F. Thermo-Magneto-Gravimetry

By virtue of being ferromagnetic, the amorphous metal core in the presence of a magnetic field experiences a motive force, which can be exploited analytically. TMG analysis is carried out in a standard thermo-gravimetric analysis device with the addition of a magnetic field introduced in the sample chamber, as diagrammed in Figure 8. Thus, the force exerted on the load cell is comprised of the force of gravity on the composite, and the magnetic force as well.

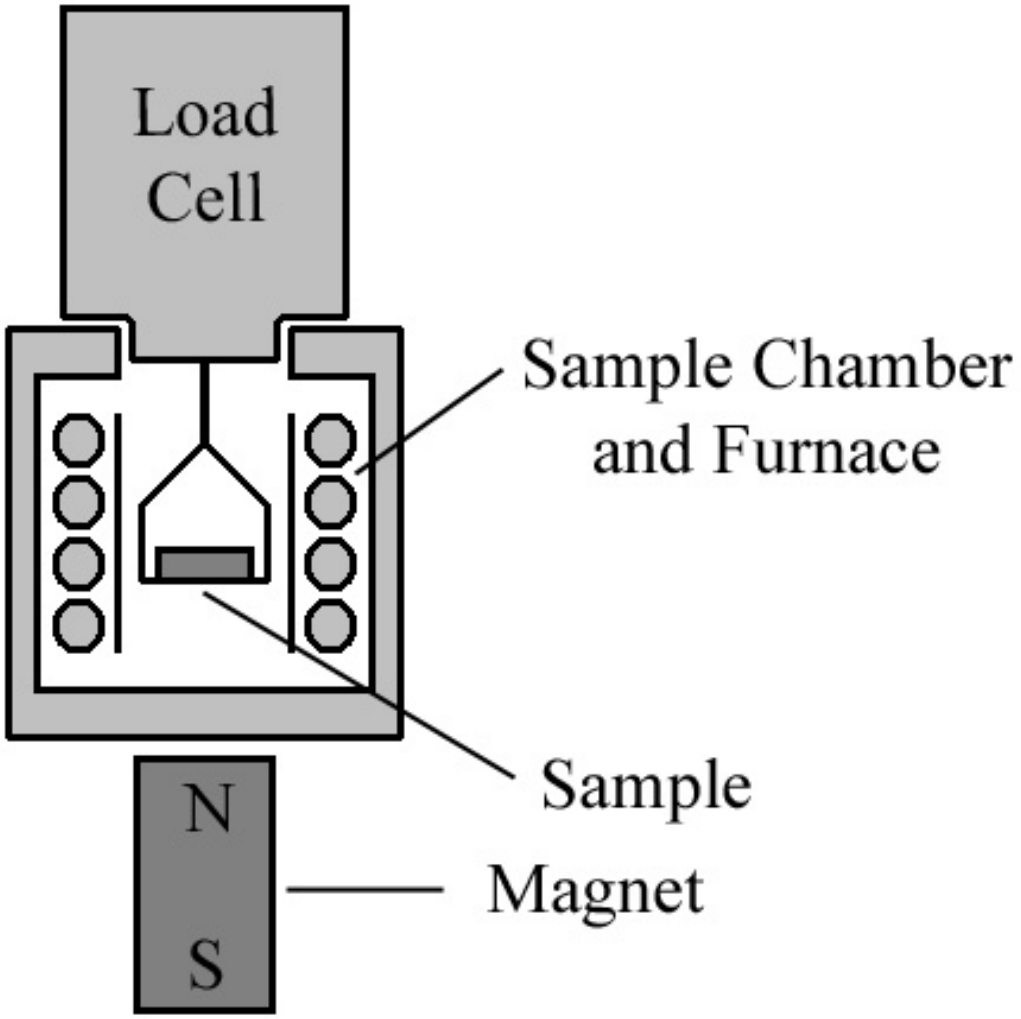

Figure 8. Schematic of a thermo-magneto gravimetric device.

Because the GCAM fibers are primarily inert in terms of weight change below 600°C, the signal response over the temperature sweep is essentially only due to the changes in the magnetic properties of the material. A TMG curve is shown in Figure 9, showing the changes in magnetization.

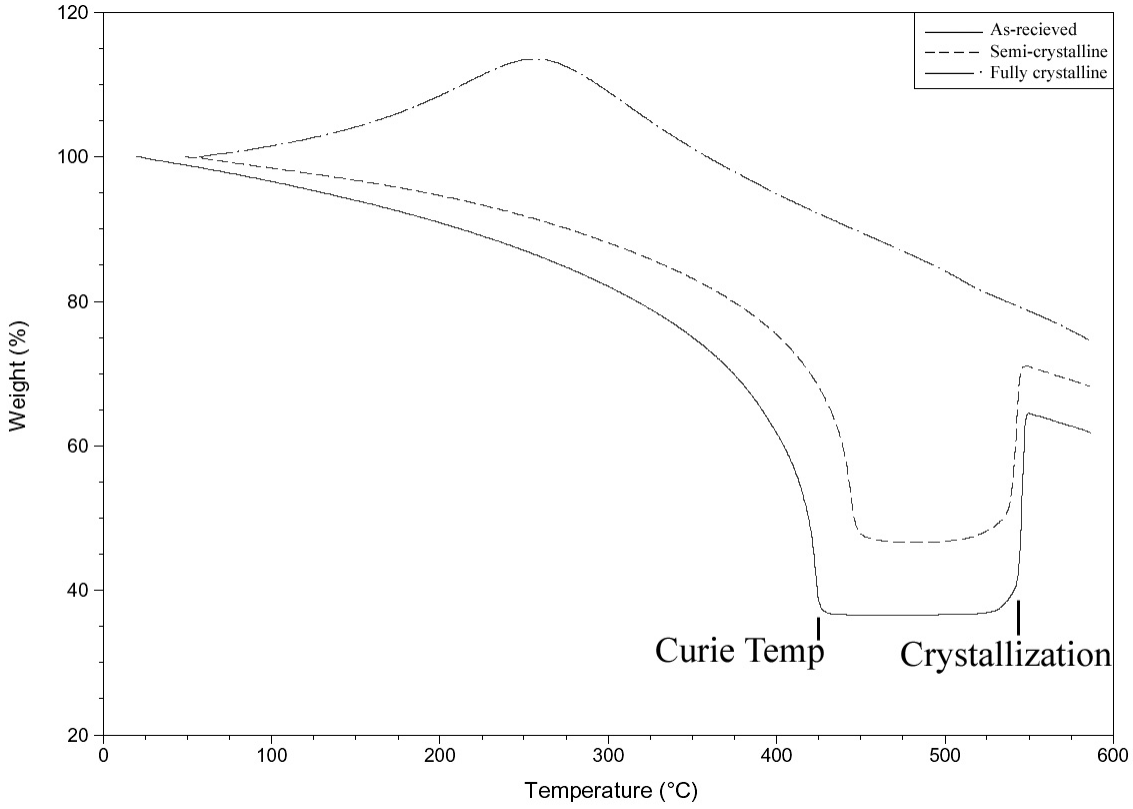

Figure 9. A thermo-magneto-gravimetric curve showing the manetization of GCAM fiber over a temperature range covering the Curie temperature, and crystallization.

The data can be used to measure the Curie temperature of the amorphous metal core, values of which are listed in Table III. The Curie temperature represents the point at which the thermal energy of the material causes the magnetic domains to become randomly oriented rather than aligned, and the material changes from ferromagnetic to paramagnetic. When this happens, the signal force only consists of the original mass of the sample, which does not change with temperature, causing the low and flat region of the curve, in this case the sample mass accounts for only 35% of the initial force exerted on the instrument. This paramagnetic region, between the Curie temperature and crystallization offers an interesting engineering state, a condition of use where the iron

alloy core is amorphous but effectively non-magnetic. Upon crystallization, FeSiB samples return to a ferromagnetic state, while CoFeSiB samples appear to remain paramagnetic, as seen in Figure 10. Fully crystalline iron compositions do not have a curie temperature in this temperature range. The Curie temperature shift during partial crystallization could be an important metric in determining the degree of crystallization.

Table III. Curie Temperatures of GCAM Samples

Composition	**Curie Temp (°C)**
As Received FeSiB	426
Semi-Crystallized FeSiB	447.5
As-Received CoFeSiB	319
Fully crystallized CoFeSiB	341.5

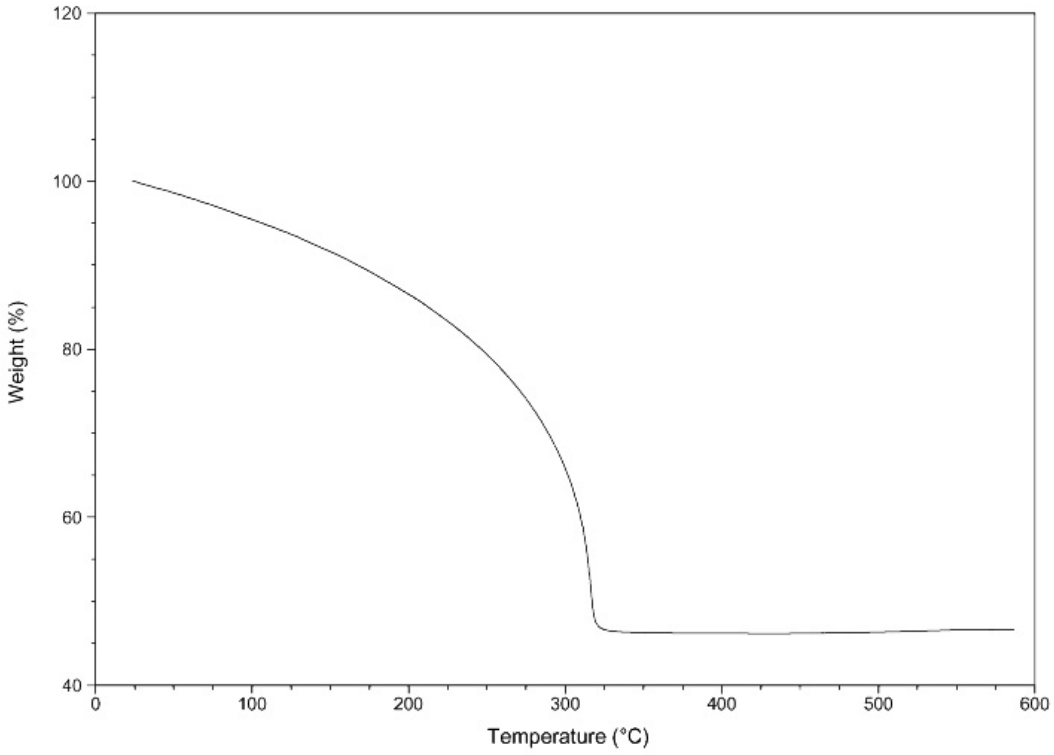

Figure 10. TMG curve for CoFeSiB fiber showing no return to ferromagnetism after crystallization.

G. Resistive Heating

A study was made to investigate the material's mechanical response to current induced heating of the GCAM fiber. An apparatus was constructed such that a length of fiber could be lightly held in position with a voltage applied, using clamping test leads, and a traveling microscope was used to monitor the change in length of a segment of the fiber, as shown in Figure 11. Other methods used to determine the thermal expansion of glass fibers could not be used, primarily due to the thermal conductivity of the GCAM core. Resistive heating ensured that the temperature would be consistent throughout the fiber length, while allowing visual access to measure length changes. Electrical contact was made by carefully removing the glass covering at two points and attaching test leads, which also served to apply a miniscule tensioning force on the fiber to hold it straight and in place. Input power was calculated from current and voltage at the supply.

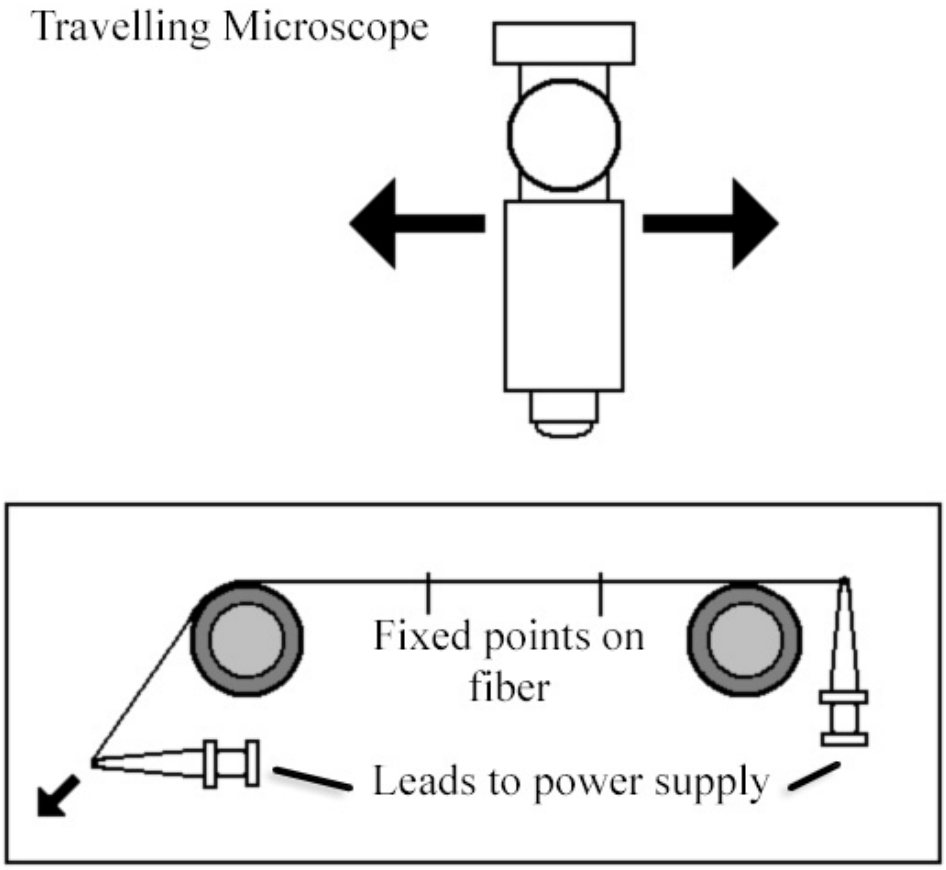

Figure 11. Schematic of the resisive heating apparatus.

The results shown in Figure 12 demonstrate that the change in fiber length is linearly proportional to the power being dissipated in the fiber. Under the assumption that the GCAM has a constant thermal expansion coefficient, the temperature of the fiber can be considered to be linearly proportional to the power dissipated in the fiber as well, allowing for the possibility of measuring the thermal expansion. Unfortunately, a consistent relationship could not be established between thermal expansion and power input, in part due to a lack of thermal reference points. The only direct measurements of temperature were room temperature equilibrium, and the melting point of tin slivers placed on the fiber. The power supply did not have the capacity to drive the temperature much above this range, but if enough current could be supplied to the fiber, the temperature would increase to the point of crystallization. Thermal indexing waxes were investigated, but the large grain size, the localized heating, and surface tension of the wax

prevented measurements of any useful accuracy. To measure the expansion coefficient using resistive heating, the fiber would have to be coated in a series of insulating layers with varying (low, known) melting points, in order to insure a uniform radial heat distribution, and calibrate exact temperatures with power input.

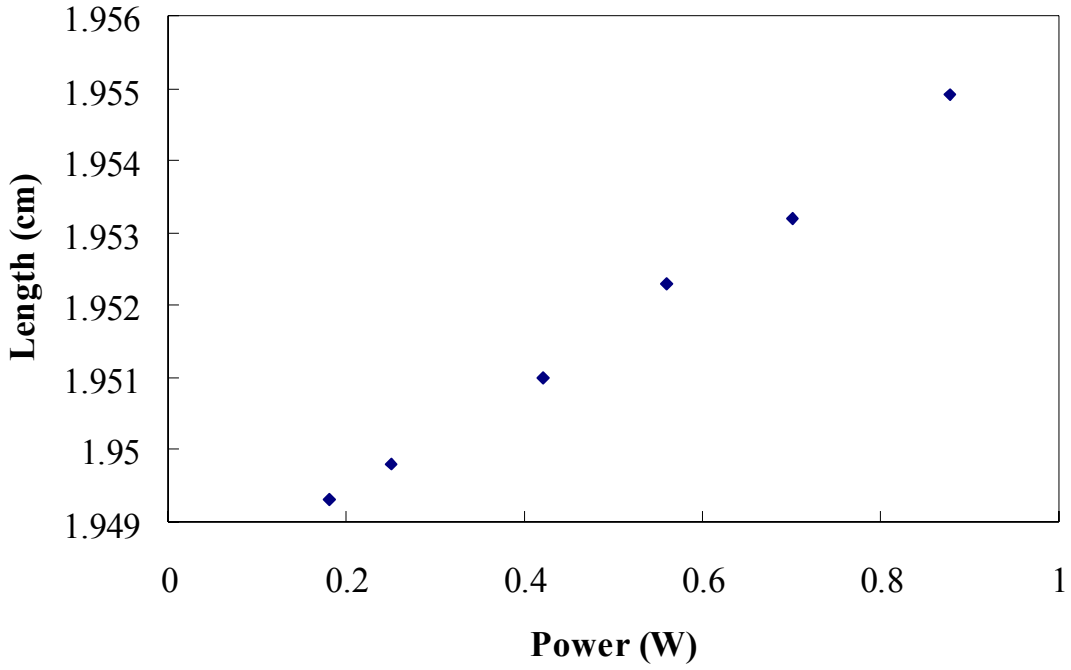

Figure 12. Graph shoing the linear change in length with power dissipated in fiber.

Figure 13 shows that cobalt based fibers also exhibit linear expansion with dissipated power, as would be expected. If the expansion curve is superimposed on two reference temperatures taken, at 25°C (equilibrium) and 232°C (melting point, tin sliver), an expansion coefficient of 3×10^{-6} can be estimated, but cannot be considered accurate without using more reference temperatures.

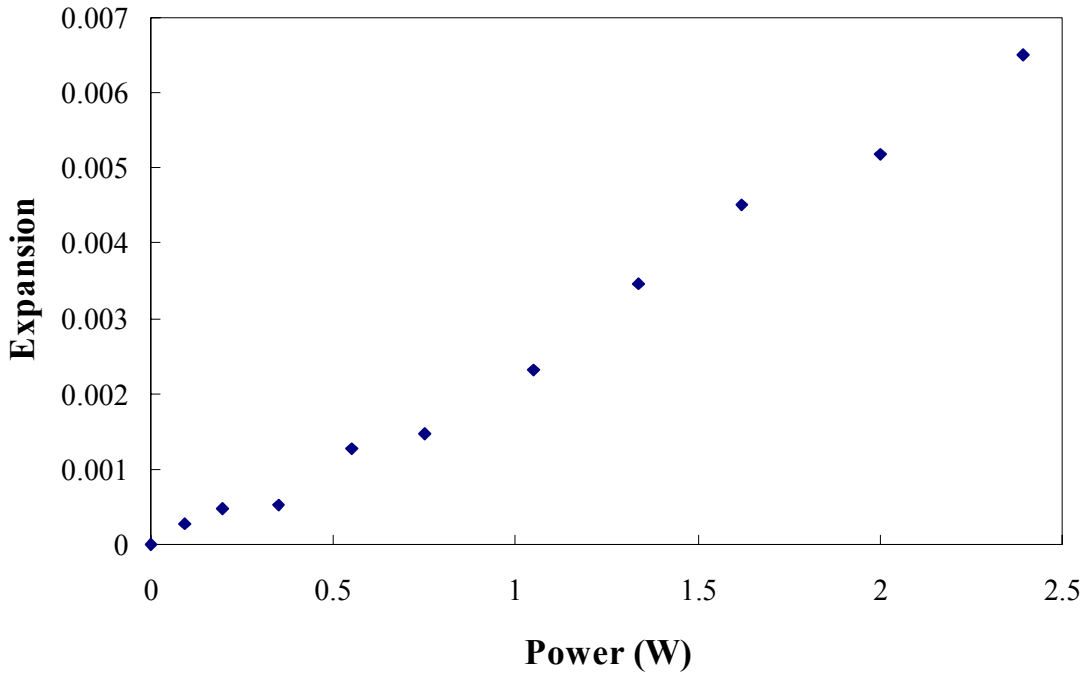

Figure 13. Expansion curve of CoFeSiB composition against power input.

Resistive heating is important to consider when engineering with GCAM fibers, as many magnetic properties are influenced by the temperature of the composite, such as GMI and magnetostrictive effects.[21] If a device utilizes the temperature dependant properties of the material, electrical control over the temperature would be very useful.

H. Magnetic Harmonic Resonance

When subjected to an oscillating magnetic field, GCAM fibers produce a corresponding magnetic field, as well as harmonic overtones at higher frequencies. These harmonics vary in intensity according to the composition and treatment of the material. The magnetic harmonics were measured by a system using a signal generator, field and pickup coils, a frequency analyzer, and an oscilloscope; a schematic is shown in Figure 14. The coils were coaxial, into which a single fiber was placed, approximately twice as long as the longer coil to avoid end effects. A 1kHz signal was applied at 150 mV, and FeSiB GCAM samples were tested; as-received, glass-removed, and semi-crystallized. A bar graph of the harmonic response is shown in Figure 15. It can be seen

that in the glass removed and semi-crystallized fibers, the even harmonics drop out nearly to background noise levels, whereas the odd harmonic strength remains comparable to, or exceeds that seen in the as-received samples.

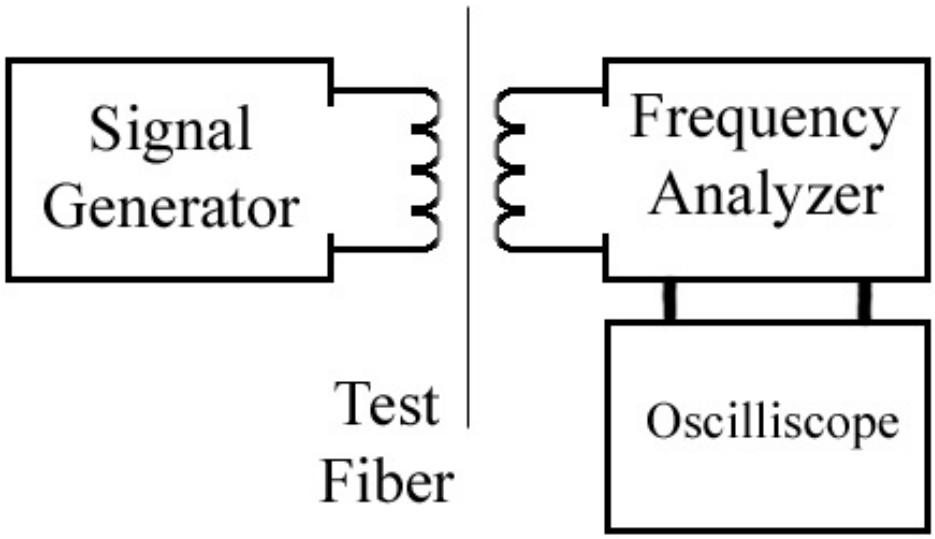

Figure 14. Diagram of the harmonic analysis setup.

Therefore, it may be postulated that the even harmonics observed in the as-received material are related to the stresses in the amorphous metal core produced by the glass covering, since both the glass removal and partial crystallizations cause the majority of those stresses to be relieved. Some differences are seen between the glass-removed sample and the semi-crystallized one, with the glass-removed fiber showing larger harmonics at higher order odd harmonics.

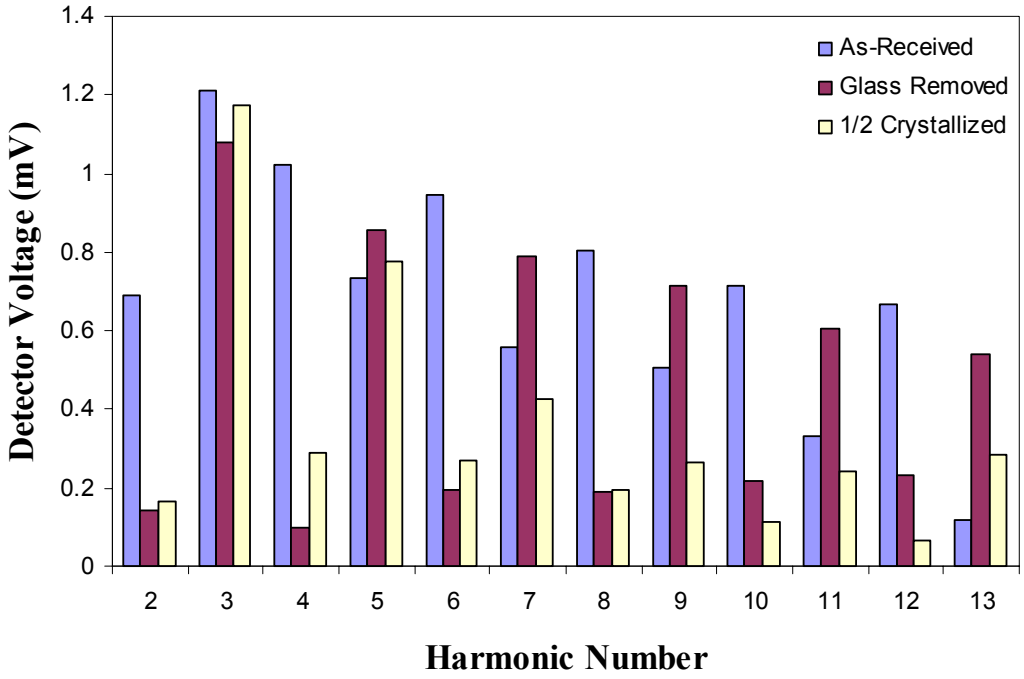

Figure 15. Bar graph showing the magnetic harmonic response of $Fe_{77.5}Si_{7.5}B_{15}$ composition GCAM fiber at 1kHz.

The frequency spectrum was difficult to stabilize for the iron based composition, very susceptible to external strains on the fiber, and its position within the detector. This might indicate that the magnetic response of the iron based fiber is more dynamic, and more sensitive to changes in internal stress than that of other compositions .

I. Strength Testing

One characteristic of the GCAM fiber material is the high values for mechanical strength observed in the as received material. Upon heat treatment and partial crystallization however, strength is notably diminished. The fiber strengths were tested using a load cell and a mechanical advance, much like large-scale mechanical testers. Samples were prepared for testing by attaching lengths of fiber to rectangular paper scaffolds. The paper serves two purposes; first to protect the fiber prior to testing and permit early preparation of the fiber, and second provide the fiber with an adequate surface to be gripped by the sample clips. Once in place, the two arms of the paper frame

are cut, and the fiber is free to be tested. A Weibull plot for as-received and semi-crystalline fibers is shown in Figure 16. It is interesting to note that not only is the partially crystallized fiber weaker, it appears to have two failure modes, widely separated, most likely attributable to handling damage.

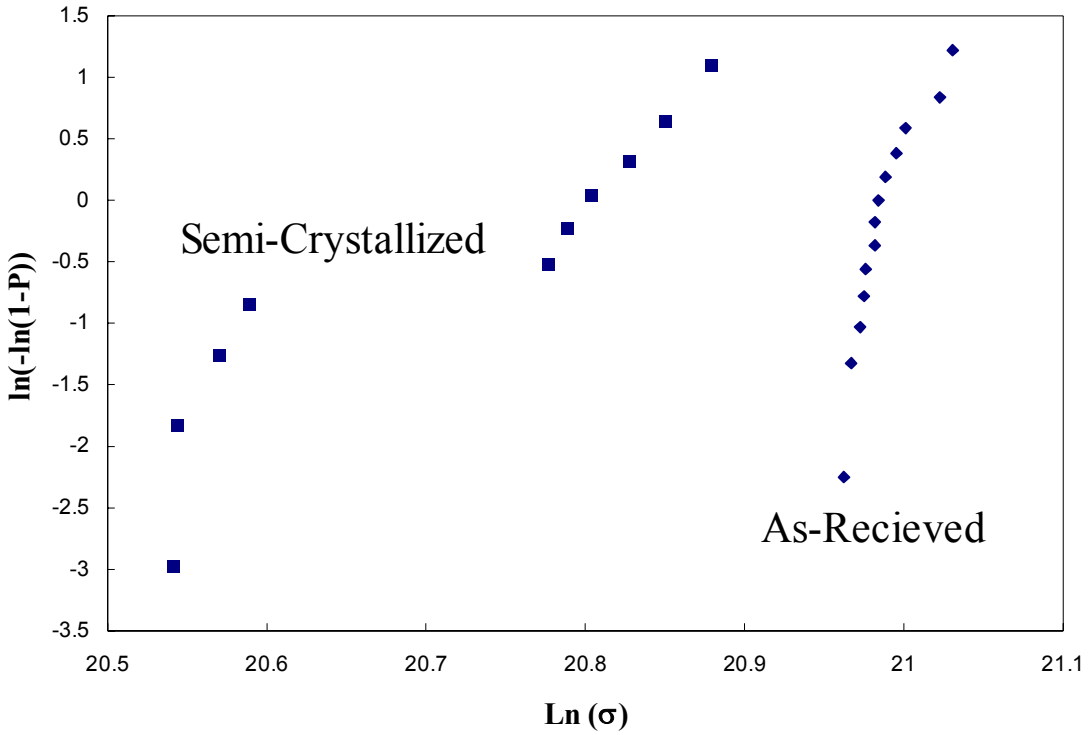

Figure 16. Weibull plot for FeSiB fiber, semi-crystalline and as-received.

The as-received samples showed an average tensile strength of 1.3GPa, while the partially crystallized fibers had an average tensile strength of only 1GPa. The standard deviation of strength values is much larger for the crystallized material; 135MPa as compared to only 32MPa. This means that a sample that has been partially crystallized will be 10-40% weaker than a standard fiber. The Weibull plot exhibits a bimodal distribution of failure stress on the fiber, indicating that the fibers fracture in two different manners. Typically, characteristically weaker samples can be attributed to damage incurred during handling, which introduces flaws into the surface of the sample, from which catastrophic failure can originate. Because the partially crystalline samples were not handled differently than the as-received ones, damage to the glass may be discounted.

However, if during heat treatment and crystallization the core and covering became separated, the glass cover would become very fragile and subject to fracture during handling, causing damage to the load bearing metal core.

Simple observation and handling of the crystallized material shows that the strength of the fiber is by far much weaker than the as-received material when subjected to stresses other than tension. Bending, crushing, and slicing failures occur with many times the ease of those performed on an un-crystallized sample.

J. Handling, Preparation, and Safety

Due to the small dimensions, stiffness, and magnetic nature of the GCAM fiber, some specialized techniques should be used during handling so that the material can be controlled and to avoid injury.

To prepare DSC samples, the fiber must be chopped into short lengths (<5mm) and captured in an aluminum sample pan with a lid. A length of fiber is wrapped around a 3cm form and cut once so that a number of shorter fibers are aligned to be cut. Being magnetic, short bits of chopped fiber will stick to steel scissors; ceramic scissors would solve this problem. When being cut, the fiber segments are collected on a stiff piece of plastic behind which is placed a magnet to attract the material. The fibers are then maneuvered so that a sample pan will fit over top of them. A second magnet and plastic shield are placed over the pan, and the first magnet is removed, causing the fiber to be attracted to the bottom of the sample pan, at which point a lid may be fitted into place.

GCAM fibers are also susceptible to static electrical charges, which can make handling somewhat difficult in the presence of some materials, particularly plastic bags.

Because handling requires maximum dexterity, fibers must be manipulated with bare hands, clean and dry. However, this increases the likelihood of getting slivers. The high aspect ratio of fiber segments allows them to penetrate skin quite easily, causing irritation; tweezers and a magnifying glass should be on hand. Glass coated fiber should not be allowed to slide over exposed skin with any more than a slight degree of force, as the glass covering can tend to splinter off, creating an irritating compound sliver injury that cannot be removed. This danger is especially present in crystallized fiber.

As received fiber will always attempt to straighten when coiled or otherwise manipulated, holding the ends in place with scotch tape is simple and effective. After annealing, the fiber will tend to retain the form it was in during treatment. In the case of a coil, this can lead to kinking, knotting, and tangles, causing difficulties if the fiber is weakened.

K. Scanning Electron Microscopy

A number of samples were prepared for SEM study, before and after crystallization and acid treatments. Figure 17 shows a fiber treated in an elevated temperature sulfuric acid atmosphere. To the left of the picture, a smooth, undamaged segment of the glass coating can be seen, which continues into the body of the fiber. This observation would seem to indicate that sulfuric acid attacked the glass chemically from the fiber end. It is a common phenomenon for Pyrex-type glass to develop a thin surface layer of a high silica composition during forming, due to boron loss to the environment. This silica layer appears to have protected the fiber from acid attack except at the fracture surface where the bulk glass composition was exposed, and corroded the glass cladding back from there. Fibers treated with hydrofluoric acid show a different behavior; the immersion line where the fiber met the liquid acid is well defined, as the acid readily dissolves silica glass.

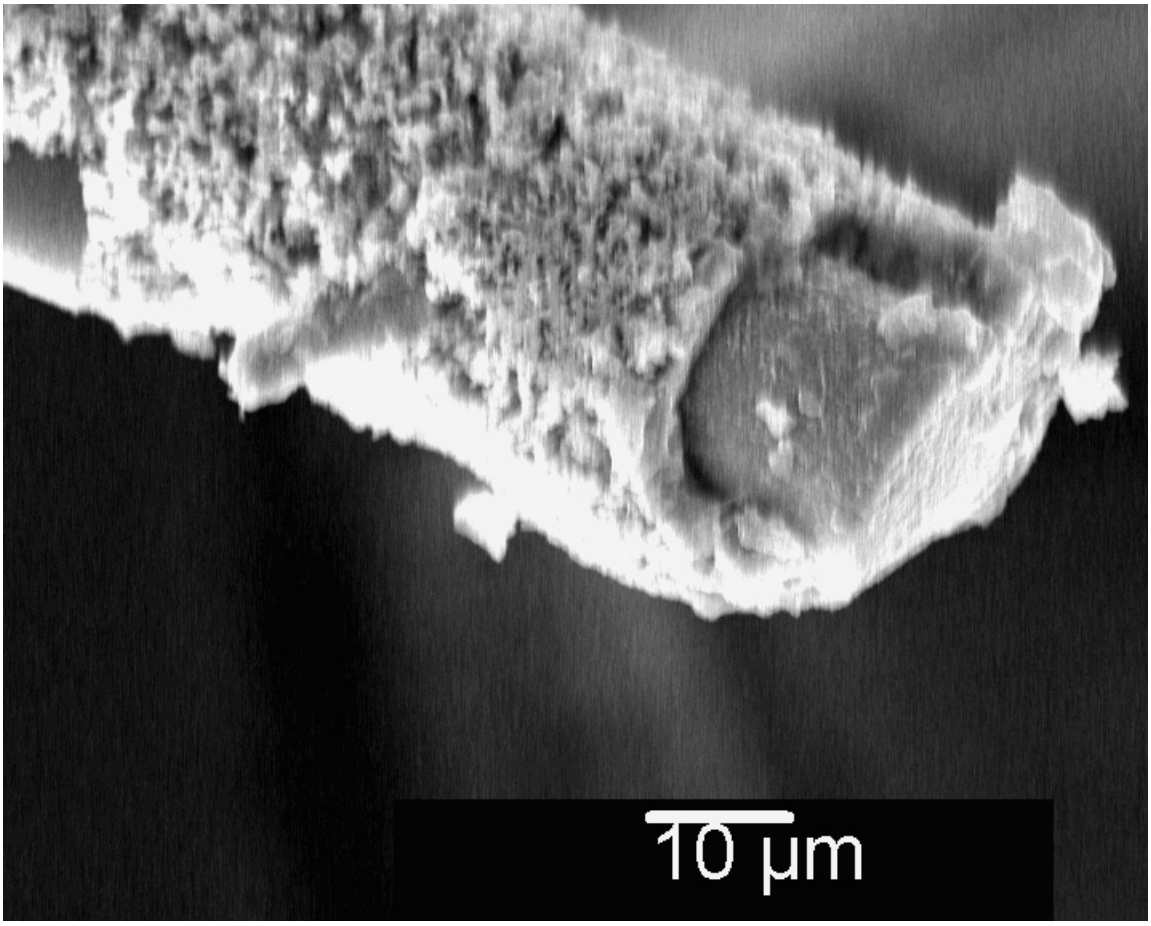

Figure 17. SEM micrograph of a sulfuric acid treated fiber.

Of the samples observed, the nominal dimensions of the fiber seem to be accurate for the most part. Measurement was not perfectly precise due to the difficulty of polishing fibers end-on, even when embedded in epoxy. The glass coating tends to fracture and chip out, and the metal core can be smeared somewhat by the polishing wheel. A good example of a fiber cross-section is shown in Figure 18, also an example of semi-crystallized fiber.

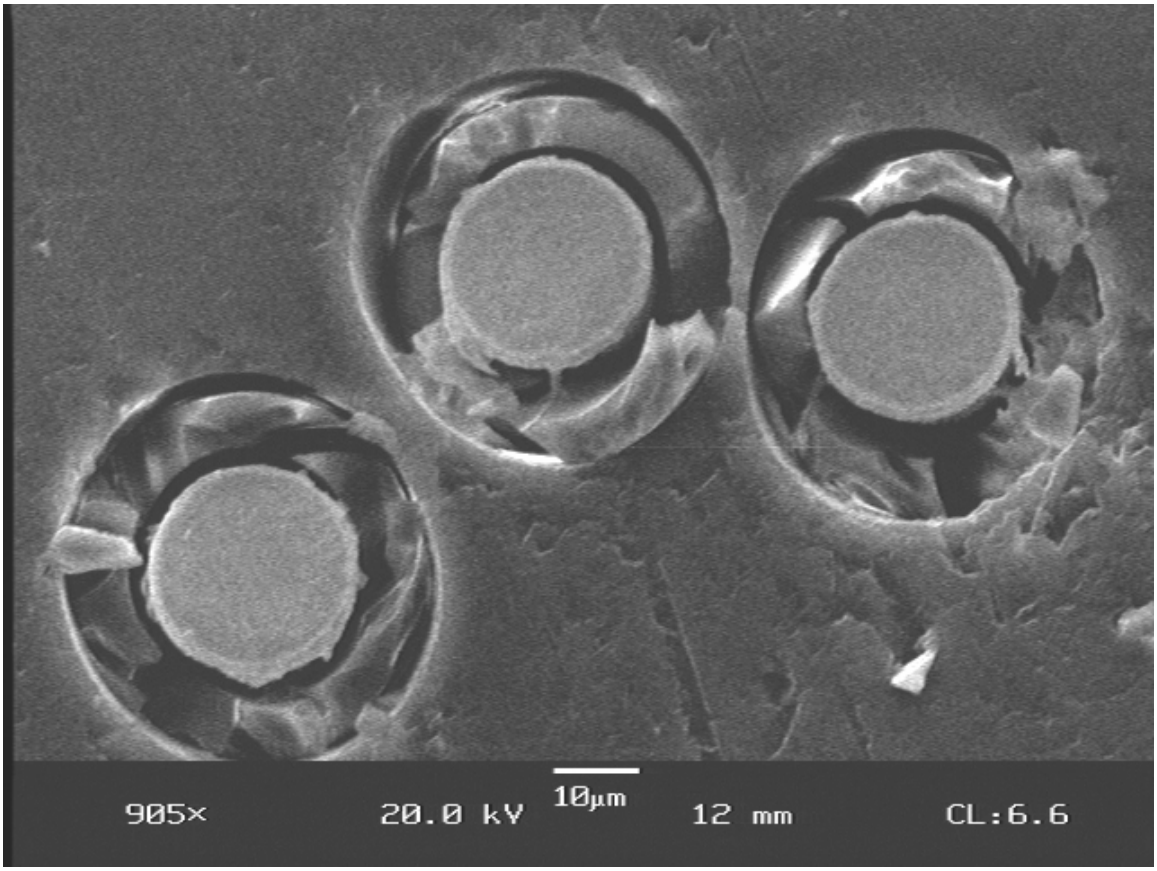

Figure 18. SEM micrograph showing GCAM fiber cross-sections.

A group of semi-crystalline fibers were cross sectioned, etched in 2M sulfuric acid for 10 minutes in order to observe any grain structure that may have developed during heat treatment. Several such fibers are shown in Figure 19, demonstrating a nano-crystalline character of the metal core. It may be noted that in some samples the remaining structure suggests two interconnected phases, as in images (a) and (b), while others show one phase isolated within another; (c) is etched, while (d) is an un-etched surface fractured prior to heat treatment. The differences in structure are likely due to subtle differences encountered during heat treatment.

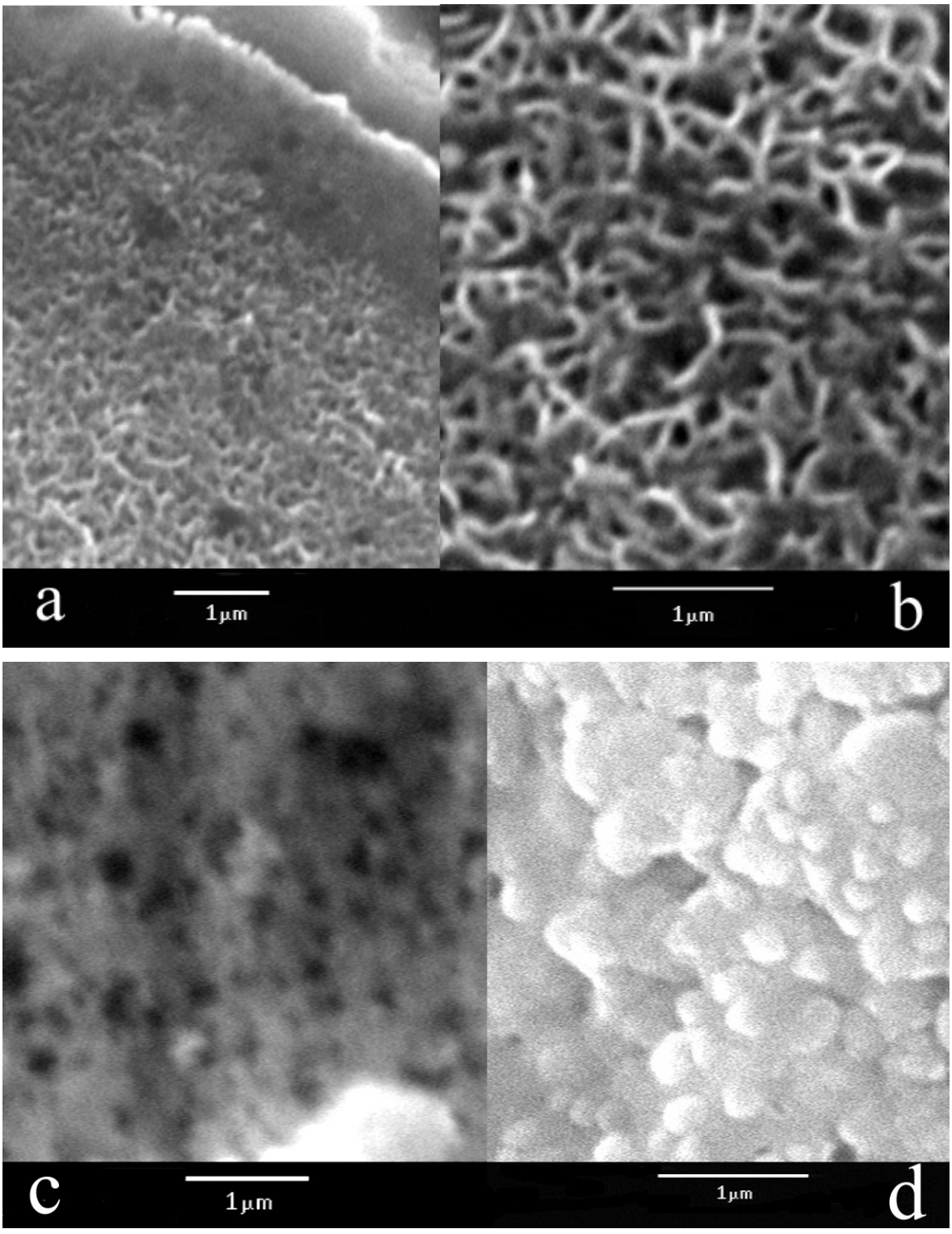

Figure 19. Images of the cores of semi-crystalline fibers, showing nanoscale structure.

It has previously been proposed that the first crystallization (lower temperature) peak formed a simple iron phase with little or no silicon content. If such a

crystalline iron phase were being dissolved, the ratio of silicon to iron would appear to increase in the etched material. Experimentally however; the ratio of silicon to iron is seen to decrease in the etched material, indicating that the dissolving phase contains more silicon than does the remaining material.

Energy Dispersive Spectroscopy was performed on two partially crystallized core samples, one as-received, and the other etched. EDS measures X-rays that are emitted when a sample is bombarded with accelerated electrons, as in a Scanning Electron Microscope. Individual elements then emit X-rays at specific and characteristic frequencies. A typical EDS spectrum is seen in Figure 20.

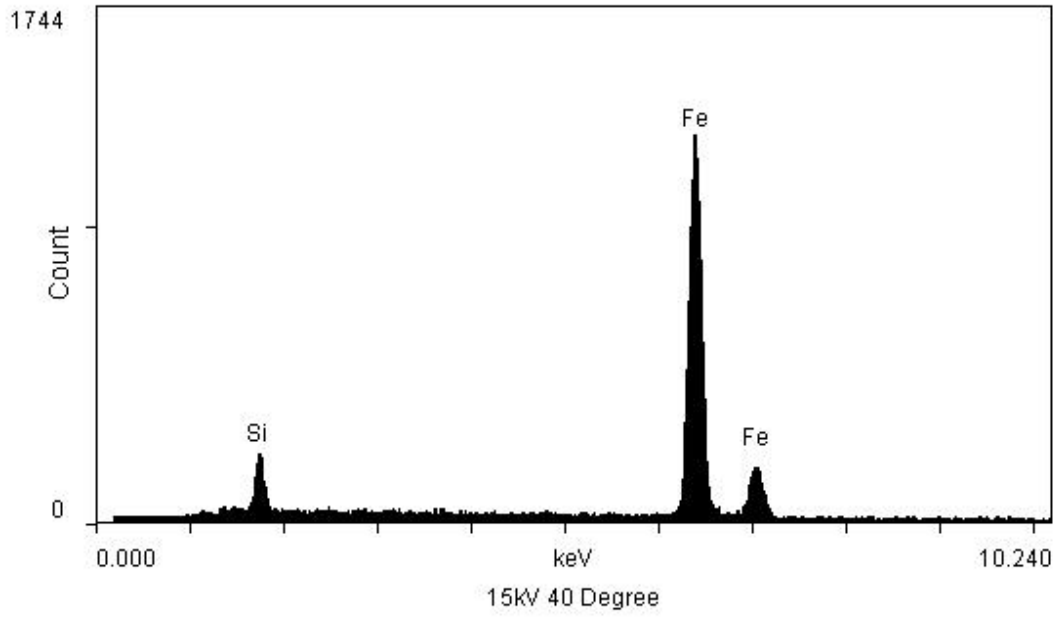

Figure 20. EDS spectrum of FeSiB composition fiber.

The number of X-rays counted can then be related to the relative concentrations of elements within the sample. Table IV shows ratios of the primary silicon and iron count peaks observed between the etched and un-etched samples, and indicates a lower silicon content in the etched samples. Two pairs of etched and un-etched semi-crystalline fibers were tested to confirm the relationship.

Table IV: Ratio of Iron to Silicon X-ray Count Peaks

	Etched	Un-etched
Trial 1	83	31
Trial 2	72	41

Although the overall composition of the un-etched samples is known, the specific composition of the etched material cannot be determined using EDS, only that the remaining material has a lower silicon content. This is due to uncertainty over the etching depth profile, that is, how far into the sample material has been removed. X-rays are produced to a depth of at least 1μm, and the depth of etching is uncertain.

What is indicated by this is that the phase most susceptible to sulfuric acid corrosion contains a higher relative amount of silicon. Fibers treated in a sulfuric acid vapor environment, at temperatures sufficient to cause crystallization, are observed to have well preserved and reasonably un-corroded cores relative to the glass cover, as seen in Figure17. This implies that the first crystallization is forming a high iron content phase that is not dissolving in sulfuric acid as readily as the amorphous phase. However, regardless of which phase is crystalline, it may be concluded that the higher silicon content raises the H_2SO_4 solubility of one phase relative to the other.

One of the considerations that must be made when crystallization of amorphous materials is under investigation is the fact that there is a negative volume change associated with the transition from a disordered to a crystalline structure. When this happens in a GCAM, the core attempts to contract when it crystallizes, but is already under tension in dynamic equilibrium with the glass cladding. Thus, the additional volume change from crystallization must be compensated for. Observing crystallized fibers under the electron microscope, it may be noted that the glass covering remains unbroken, the metal core is neither hollow, nor porous, and the fiber remains conductive. Thus it may be expected that the core necessarily separates from the glass to some degree. This may be observed in Figure 21, where metal polishing debris has filled in a ring about the core. More defined separation can also be seen in Figure 18.

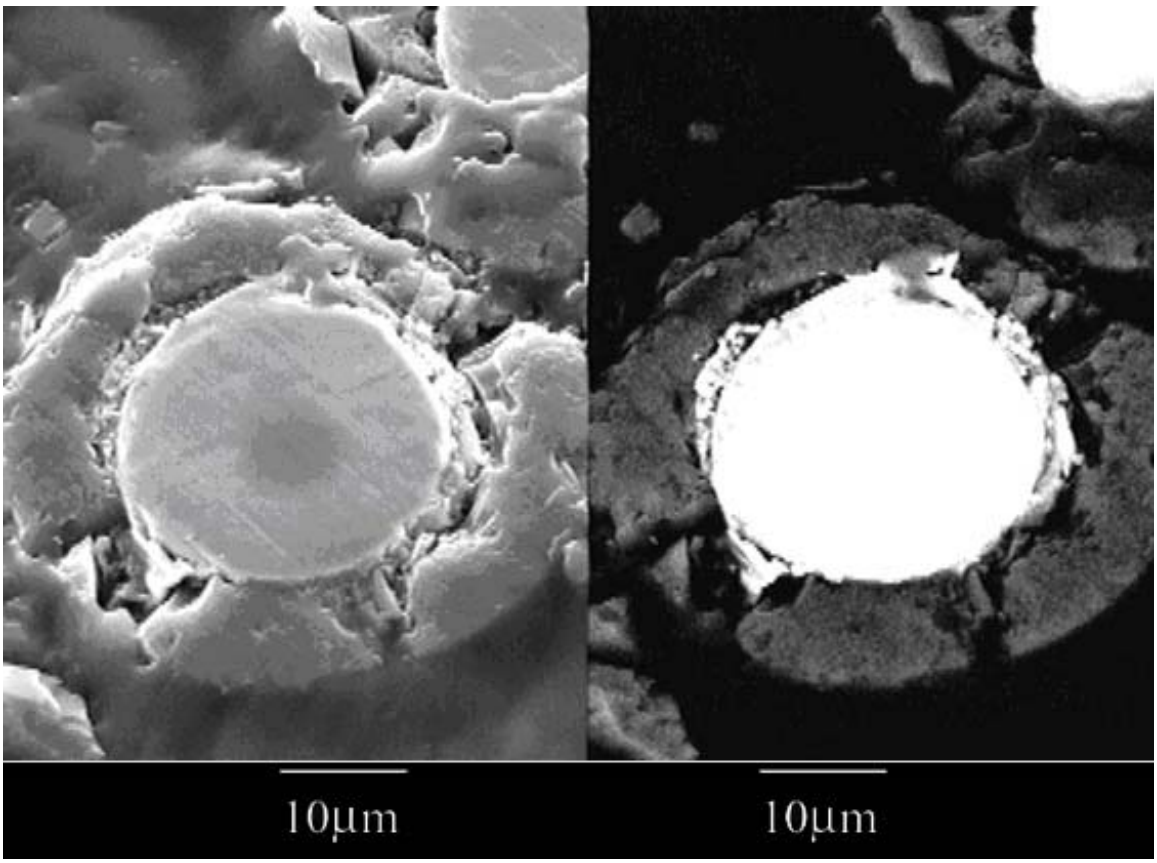

Figure 21. Normal and BSE images showing separation of the metal core from the glass, and backfilling with polishing burr.

III DISCUSSION

A. Core-Cladding Separation

The separation between the metal core and the glass upon crystallization indicates several things about the composite. First, the bond between the core and cladding must be weaker than the bulk materials themselves. This implies that even in an as-received fiber, the failure characteristics will be controlled in part by the glass-metal bonding. Secondly, the de-bonding of the layers severely compromises the overall strength of the fiber. Without the compressive stress in the glass, the cladding is very fragile and subject to failure, and without the protective covering, the metal is susceptible to surface damage and failure. Third, the fiber no longer functions as a composite, but rather two adjacent elements, thus they are unable to support each other mechanically or transfer and distribute stress, leading to higher stress concentrations and failure. This is supported by the observation that crystallized fibers are many times weaker than the un-treated counterparts when exposed to non-tensile stresses.

When considering the Weibull plot of the tensile strength measurements in Figure 15, two distinct regions of the graph stand out; a somewhat weaker and more broadly spaced group of failure points, and a much weaker, but closely spaced group. Since damaged samples almost always exhibit lower strength values, it may be safely assumed that the weaker samples were subjected to handling damage during testing. However, the closely spaced distribution of breaking stresses is not generally typical of damage induced failure. What may be happening is that only the glass covering is breaking off in places, weakened by the separation from the core, exposing the metal beneath. If only the metal core bears the load, the breaking load will be much lower, but the breaking stress will be miscalculated, because the cross sectional area will have changed. Recalculating the stress using these assumptions, the strength of partially crystallized fiber with no glass covering has an average strength of about 1.76GPa. This represents a lower strength than the as-received material, which exhibits strength values of approximately 3.2 GPa.

B. Double Crystallization

The DSC curve for the iron based GCAM shows two crystallization peaks that are sufficiently distinct to indicate that they represent two processes within the material. However, partial crystallization thermal treatments have shown that the second crystallization is dependant on the degree of completion of the first, raising the possibility that they are both stages in a larger, unified process. While the current work has shown that the two crystallizations can be split by careful heat treatment, no analysis has thus far shown that the variance in properties from the as-received material to the partially crystallized one is any different than would be expected from a partially completed, single crystallization. Indeed, varying hold times for heat treatment even seems to suggest that there would be a smooth transition from the amorphous to the semi-crystalline state, rather than a sharp and well defined "notch" where one crystallization has occurred completely while the second has not begun. TMGA analysis seems to offer a method of gauging the degree of the partial crystallization by noting the shift of curie temperature. As soon as the primary crystallization begins, even if it does not proceed to completion, the secondary crystallization is diminished slightly, and shifts to a lower temperature. Thus, even if the DSC peaks seen are caused by the formation of two different crystalline phases, the occurrence of the second is inextricably tied to the occurrence of the first, and will begin to proceed as soon as (but not until) the first has begun. Whether or not the two crystallizations belong to different phases, they interrelated and not mutually independent. This means that there can never be a true "split crystallization," rather only a partial crystallization in which the majority of the crystallized material is of one composition, and a minority of the other. A much more detailed study would have to be done in order to determine the exact variation of properties from the amorphous to the crystalline state.

IV SUMMARY AND CONCLUSIONS

A. Crystallinity and Mechanical Strength

As previously noted, upon being crystallized, partially or fully, the fiber looses a tremendous degree of mechanical durability, even if the tensile strength only diminishes by 25%. Therefore, it must be expected that crystallized fibers will not be able to be incorporated into products that will subject the fiber to mechanical stress, as would a standard GCAM fiber. For example, documents, money, tamper-proof tape would all preclude the incorporation of the fiber by virtue of their softness and flexibility. Any device that uses crystallized fiber to encode information must be rigid enough to protect the fiber under normal use. If a single fiber is encoded with localized zones of crystallization, those points will be a weak link. On the other hand, if the method of detection is dependant only on the mass of material present, and not the length of fibers, fiber fracture would have no consequence in terms of detection.

If GCAM fibers are used in applications where a product is being handled, much care must be taken to prevent fiber from coming into contact with exposed skin, as explained previously in comments on safety and handling.

B. Nano-Crystallinity

The nano-scale structure observed in the partially crystallized amorphous metal cores of GCAM fibers offer new and previously unexplored potentials for application. The nano-crystalline surface of a glass-removed fiber has the possibility of changing interfacial reactions drastically when used in a variety of environments. Furthermore, the internal damage incurred during heat treatment effectively negates any structural integrity of the glass cover, which would have to be removed prior to use in any case.

C. Resistive Heating

The electrical conductivity of GCAM fibers offers an intriguing method of control on the small scale of the material. Control over the temperature of the fiber relative to its environment, and the associated change in dimensions, enhance the potential for

implementation of the fiber in devices. Given a sufficient supply of power, it may be expected that GCAM fibers may be crystallized electrically. If such is the case, the method should prove to have a higher degree of precision in the heating process, as opposed to conventional heating methods.

D. Magnetic Resonance

The magnetic response of the metal core is important to understand, especially with respect to the changes that occur when the fiber is crystallized or the glass covering removed. Some methods of detection may be developed that are dependant on specific harmonic profiles, and if those profiles can be changed, fibers could cease to be detectable, or change their characteristic signal, useful ideas when developing detection systems based on the GCAM material.

E. Future Work

The partial crystallization behavior needs to be studied in much more detail, so that sufficient control can be made on the crystallization structure of the metal core, that is, to determine the specifics of how thermal treatment influences the interconnectivity of the crystallized structure.

There are many opportunities for further study of GCAM composites, most concerning the alteration of the glass covering compositionally. The tolerances of formation must be investigated in order to evaluate the flexibility of viscosity profiles and transition temperatures during fiber drawing. In order to study alternative glass coverings, or investigate different fiber geometries, local access to a fiber production apparatus is critical; that is, the capability of making fibers must be established before more research on the material can be adequately performed.

Some interesting possibilities for the future could include designing multiple core fibers, based on the geometry of the glass perform tubing used during manufacture, perhaps two parallel metal cores or more, or even a glass core within the metal. Or, using a thick glass layer, a small metal core could be dissolved from within the cladding, producing a hollow fiber with micro-meter dimensions.

REFERENCES

1. H. Chiriac and T.A. Ovari, "Amorphous Glass-Covered Magnetic Wires: Preparation, Properties, Applications," *Prog. Mater. Sci.,* **40** [5] 333-407 (1997).

2. H. Chiriac, "Preparation and Characterization of Glass Covered Magnetic Wires," *Mater. Sci. Eng., A,* **A304-306** [1-2] 166-71 (2001).

3. A. Zhukov, M. Vazquez, J. Velazquez, A. Hernando, and V. Larin, "Magnetic Properties of Fe-Based Glass-Coated Microwires," *J. Magn. Magn. Mater.,* **170** [3] 323-30 (1997).

4. H. Chiriac and T.A. Ovari, "Magnetic Properties of Amorphous Glass-Covered Wires," *J. Magn. Magn. Mater.,* **249** [1-2] 46-54 (2002).

5. H. Chiriac, T.A. Ovari, G. Pop, and F. Barariu, "Amorphous Glass-Covered Magnetic Wires for Sensing Applications," *Sens. Actuators, A,* **59** [3] 243-51 (1997).

6. G.F. Taylor, "A Method of Drawing Metallic Filaments and a Discussion of Their Properties and Uses," *Phys. Rev.,* **23** [1] 655-60 (1924)

7. H. Wiesner and J. Schneider, "Magnetic Properties of Amorphous Fe-P Alloys Containing Ga, Ge, and As," *Phys. Status Solidi,* **26** [1] 71-5 (1974).

8. M. Neagu, H. Chiriac, M. Vasquez, F. Borza, and T.A. Ovari, "Saturation Magnetostriction of Co-Rich Glass-Covered Amorphous Wires," *J. Magn. Magn. Mater.*, **254-5** [1-3] 472-4 (2003).

9. H. Chiriac and T.A. Ovari, "Switching Field Calculations in Amorphous Microwires with Positive Magnetostriction," *J. Magn. Magn. Mater.*, **249** [1-2] 141-5 (2002).

10. H. Chiriac, M. Neagu, M. Vazquez, T.A. Ovari, and E. Hristoforou, "Stess Dependence of the Saturation Magnetostriction in $Co_{68.15}Fe_{4.35}Si_{12.5}B_{15}$ Glass-Covered Amorphous Wires," *J. Magn. Magn. Mater.*, **249** [1-2] 122-5 (2002).

11. L. Kraus, Z. Frait, K.R. Pirota, and H. Chiriac, "Giant Magnetoimpedance in Glass-Covered Amorphous Microwires," *J. Magn. Magn. Mater.*, **254-5** [1-3] 399-403 (2003).

12. R. Germano and L. Lanotte, "Application of Magnetoelastic Waves for Sensors of Displacement," *Sens. Actuators, A,* **59** [1-3] 337-41 (1997).

13. R. Germano, G. Ausanio, V. Iannotti, L. Lanotte, and C. Luponio, "Direct Magnetostriction and Magnetoelastic Wave Amplitude to Measure a Linear Displacement," *Sens. Actuators, A,* **81** [1-3] (2000).

14. H. Chiriac, C.S. Marinescu, T.A. Ovari, and M. Neagu., "Sensor Applications of Amorphous Glass-Covered Wires," *Sens. Actuators, A,* **76** [1-3] (1999).

15. H. Kissinger, "Reaction Kinetics in Differential Thermal Analysis," *Anal. Chem*., **29** [11] 1702-6 (1957).

16. H. Kissinger, "Variation of Peak Temperature with Heating Rate in Differential Thermal Analysis," *J. Res. Natl. Bur. Stand.* **57** [4] 217-9 (1956).

17. P. Altuzar and R. Valenzuela, "Avrami and Kissinger Theories for Crystallization of Metallic Amorphous Alloys," *Mater. Lett.,* **11** [3-4] 101-4 (1991).

18. D.W. Henderson, "Thermal Analysis of Non-Isothermal Crystallization Kinetics in Glass Forming Liquids," *J. Non-Cryst. Solids,* **30** [3] 301-15 (1978).

19. H. Wang, Y. Gao, Y. Ye, G. Min, Y. Chen, and X. Teng, "Crystallization Kinetics of an Amorphous Zr-Cu-Ni Alloy: Calculation of the Activation Energy," *J. Alloys Compd.,* **353** [1-2] 200-6 (2003).

20. G. Ruitenberg, E. Woldt, and A.K. Petford-Long, "Comparing the Johnson-Mehl-Avrami-Kolomogorov Equations for Isothermal and Linear Heating Conditions," *Thermochim. Acta,* **378** [1-2] 97-105 (2001).

21. L. Kraus, M. Knobel, S.N. Kane, and H. Chiriac, "Influence of Joule Heating on Magnetostriction and Giant Magnetoimpedance Effect in a Glass Covered CoFeSiB Microwire," *J. Appl. Phys.,* **85** [8] 5435-7 (1999).

22. F. Johnson, P. Hughes, R. Gallagher, D.E. Laughlin, M.E. McHenry, M.A. Willard, and V.G. Harris, "Structure and Thermomagnetic Properties of New FeCo-based Nanocrystalline Ferromagnets," *IEEE Trans. Magn.,* **37** [4] 2261-3 (2001).

23. G. Ruitenberg, "Applying Kissinger Analysis to the Glass Transition Peak in Amorphous Metals," *Thermochim. Acta,* **404** [1-2] 207-11 (2003).